Nano Today 51 (2023) 101884

Contents lists available at ScienceDirect

Nano Today

journal homepage: www.elsevier.com/locate/nanotoday

High-dose paclitaxel and its combination with CSF1R inhibitor in polymeric micelles for chemoimmunotherapy of triple negative breast cancer

Chaemin Lim [a,1], Duhyeong Hwang [a,1,2], Mostafa Yazdimamaghani [a,b], Hannah Marie Atkins [b,c,d,e], Hyesun Hyun [a,b], Yuseon Shin [a,f], Jacob D. Ramsey [a], Patrick D. Rädler [b,g], Kevin R. Mott [b,g], Charles M. Perou [b,c,g], Marina Sokolsky-Papkov [a,*], Alexander V. Kabanov [a,b,**]

[a] Center for Nanotechnology in Drug Delivery and Division of Pharmacoengineering and Molecular Pharmaceutics, Eshelman School of Pharmacy, University of North Carolina at Chapel Hill, Chapel Hill, NC 27599, USA
[b] Lineberger Comprehensive Cancer Center, University of North Carolina at Chapel Hill, Chapel Hill, NC 27599, USA
[c] Department of Pathology and Laboratory Medicine, University of North Carolina, Chapel Hill, NC 27599, USA
[d] Center for Human Health and the Environment, North Carolina State University, Raleigh, NC 27695, USA
[e] Department of Population Health and Pathobiology, North Carolina State University, Raleigh, NC 27606, USA
[f] Department of Pharmaceutical Sciences, College of Pharmacy, Chung-Ang University, 221 Heukseok dong, Dongjak-gu, Seoul 06974, South Korea
[g] Department of Genetics, School of Medicine, University of North Carolina at Chapel Hill, Chapel Hill, NC 27599, USA

ARTICLE INFO

Article history:
Received 24 August 2022
Received in revised form 20 March 2023
Accepted 24 May 2023
Available online xxxx

Keywords:
High-dose therapy
Polymeric micelle
Chemoimmunotherapy
TNBC model

ABSTRACT

The presence of immunosuppressive immune cells in tumors is a significant barrier to the generation of therapeutic immune responses. Similarly, in vivo triple-negative breast cancer (TNBC) models often contain prevalent, immunosuppressive tumor-associated macrophages in the tumor microenvironment (TME), resulting in breast cancer initiation, invasion, and metastasis. Here, we test systemic chemoimmunotherapy using small-molecule agents, paclitaxel (PTX), and colony-stimulating factor 1 receptor (CSF1R) inhibitor, PLX3397, to enhance the adaptive T cell immunity against TNBCs in immunocompetent mouse TNBC models. We use high-capacity poly(2-oxazoline) (POx)-based polymeric micelles to greatly improve the solubility of insoluble PTX and PLX3397 and widen the therapeutic index of such drugs. The results demonstrate that high-dose PTX in POx, even as a single agent, exerts strong effects on TME and induces long-term immune memory. In addition, we demonstrate that the PTX and PLX3397 combination provides consistent therapeutic improvement across several TNBC models, resulting from the repolarization of the immunosuppressive TME and enhanced T cell immune response that suppress both the primary tumor growth and metastasis. Overall, the work emphasizes the benefit of drug reformulation and outlines potential translational path for both PTX and PTX with PLX3397 combination therapy using POx polymeric micelles for the treatment of TNBC.

Introduction

TNBC is characterized by low/absent levels of expression of the estrogen receptor, progesterone receptor, and the lack of overexpression of the human epidermal growth factor receptor 2 [1]. It is an aggressive disease that accounts for 15–20% of all breast cancers and is associated with poor prognosis and high recurrence rate, which annually contributes to ~5% of all cancer-related deaths in women [2]. TNBC is also known for aggressive metastasis to distant organs, which is encountered in over 40% of TNBC patients [3]. In

* Corresponding author.
** Corresponding author at: Center for Nanotechnology in Drug Delivery and Division of Pharmacoengineering and Molecular Pharmaceutics, Eshelman School of Pharmacy, University of North Carolina at Chapel Hill, Chapel Hill, NC 27599, USA.
E-mail addresses: msokolsk@email.unc.edu (M. Sokolsky-Papkov), kabanov@email.unc.edu (A.V. Kabanov).
[1] These authors contributed equally to this work.
[2] Current address: Department of Pharmaceutical Engineering, Dankook University, 119 Dandae-ro, Dongnam-gu, Cheonan 31116, South Korea.

https://doi.org/10.1016/j.nantod.2023.101884
1748-0132/

addition to a relatively mixed response to traditional chemotherapies [1,3], immune checkpoint inhibitors have relatively modest results in improving therapeutic outcomes for TNBC patients. In TNBC, the objective response rate for αPD-1 monotherapy in the metastatic setting is between 8% and 19%, with no durable clinical responses [4,5]. However, when nab-paclitaxel (but not conventional paclitaxel) and Atezolizumab (Tecentriq) that targets PD-L1 were combined, this showed improved treatment outcomes and initially obtained approval by the US Food and Drug Administration (FDA) as the new standard of care in metastatic patients with PD-L1 expression [6]. Unfortunately, Genentech later voluntarily withdrew the U.S. accelerated approval for this treatment (https://www.gene.com/media/press-releases/14927/2021–08–27/genentech-provides-update-on-tecentriq-u). Therefore, developing, new effective strategies to improve TNBC immunotherapy is highly needed.

The tumor microenvironment (TME) is a critical component of tumor growth with immunosuppressive proteins and cell populations limiting an effective anti-tumor immune response [7–10]. In TNBC, the recruitment of immunosuppressive immune cells such as myeloid derived suppressor cells (MDSCs), tumor-associated macrophages (TAMs), and regulatory T cells (T_{regs}) and B cells (B_{regs}) by the tumor is a significant impediment to the generation of an effective immune response [11]. The most prevalent antigen-presenting cells within the TME are TAMs [12,13]. They can promote breast cancer initiation, angiogenesis, invasion, and metastasis by generating an immunosuppressive TME via releasing cytokines, chemokines, and growth factors [14]. The presence of TAMs in TME is associated with poor clinical outcomes in TNBC [15–17]. Targeting the immunosuppressive TME has shown potential for improving immune checkpoint inhibitor therapy in patients [18].

The prevalence of TAMs in tumors and the potential for repolarizing to pro-inflammatory phenotype, which restores adaptive immune control of tumors, makes them an attractive target for establishing an immune-promoting TME [19]. Novel therapeutics aiming to target mechanisms promoting the survival, recruitment, polarization, and other properties associated with tumor-associated myeloid cells are currently in clinical development [20]. One strategy focuses on inhibiting the function and migration to the TME of immunosuppressive monocytes and macrophages. Colony-stimulating factor 1 (CSF-1) and its receptor, CSF-1R, play a major role in regulating the proliferation and survival of macrophages and their precursors [21]. Inhibition of CSF1R with antibodies or small molecules suppresses breast cancer growth and reverses its resistance to chemo- and radiotherapy [22–24]. Blockade of macrophage recruitment with CSF1R-signaling antagonists, in combination with paclitaxel (PTX), enhanced CD8 + T cell immunity and improved survival of mammary tumor–bearing mice by slowing primary tumor development and reducing pulmonary metastasis via T cell–mechanism [22]. A number of small molecule inhibitors of CSF-1R (Pexidartinib, RXDX-105, BLZ945, Linifanib) are currently in clinical trials for the treatment of solid tumors [20,25]. They show promise in attenuating the immune escape of tumors and potentiating the effect of CPI immunotherapy and traditional cytotoxic therapy [13]. However, no intravenous (iv) formats for these agents are currently available to improve their delivery to tumor and metastatic sites and to avoid dysphagia and other common complications of oral administration after chemo- and radiotherapy [26].

Here, we present systemic chemoimmunotherapy using small-molecule agents, PTX, one of the most important therapeutic drugs in clinical management of TNBC [27], and the CSF1R inhibitor, PLX3397 (Pexidartinib) that targets myeloid cells to enhance the adaptive T cell immunity. In a free form, these agents are very poorly soluble in water and have poor distribution to the tumors. To address the challenge of delivering lipophilic drugs to tumors, we use high-capacity POx-based polymeric micelles, a transformative technology uniquely suited to greatly improve the solubility and widen therapeutic index of such drugs. This approach transforms a disadvantage of poorly soluble drugs into an advantage by packing them into small tumor-permeating polymeric micelle nanoparticles, improving their tumor distribution and enabling high-dose therapy due to increased safety [28,29]. Our findings suggest that high dose PTX and its co-loaded combination with PLX3397 enabled in POx micelles, remodel immunosuppressive TME, induce T cell-mediated antitumor response, produce immune memory and overall show promise as chemoimmunotherapy in animal models of primary and metastatic TNBC.

Results

Preparation and characterization of drug-loaded polymeric micelles

POx-based polymeric micelle formulations containing PTX and PLX3397 were prepared using a thin film method, as previously reported [30]. In prior work, we determined that POx block copolymers can efficiently solubilize PTX (POx-PTX), forming well-defined spherical micelles in aqueous media with extremely high drug loading and increased PTX solubility of up to 40 mg/ml [31]. In the current study, we solubilized PLX3397 in POx micelles (POx-PLX). As presented in Fig. 1**(a)**, PLX3397 incorporated in the micelles with nearly no loss of the drug (98.8% LE) and at extremely high drug loading (44.1% LC). The overall solubility of PLX3397 in the micellar solution was also greatly increased to at least 20 mg/ml compared to the insolubility of the drug in water. The resulting POx-PLX micelles were spherical and extremely well-defined, with a particle size of 38 nm and PDI of 0.05, as determined by DLS. The PTX and PLX3397 combination micelles (POx-PTX/PLX) were also easily prepared by co-loading these drugs at a 1/1 (w/w) drug ratio in the POx micelles (Fig. 1**(a)**). There was little or no loss of the drugs upon loading (94.0% LE for PTX and 99.9% LE for PLX3397, respectively) and the resulting micelles also contained high amounts of drugs per polymer (the combined LC was as much as 44%; 21.2% for PTX and 22.5% for PLX3397). Like the single drug micelles, the co-loaded micelles were also spherical and well-defined (57 nm, PDI = 0.16).

For the stability studies, the micelle solutions were kept at 4 ºC for up to 4 days and then the particle size and PDI values were measured at room temperature by DLS. The single drug POx-PLX micelles aggregated at day 2, accompanied by a drastic increase in the particle size and PDI, as well as visual drug precipitation. In contrast, the combination micelles retained their small size and PDI for the entire observation period, with no drug precipitation observed (Fig. 1**(b)**). The stabilization effect was obviously due to the contribution of the PTX, as the single drug POx-PTX micelles are stable in solution for at least two weeks [32]. Previously, we demonstrated that POx-based polymeric micelles can be elongated over time from a spherical structure to worm-like structure, and the elongation process can be inhibited or stabilized by loading specific type of drugs, such as PTX [33,34]. PTX contains numerous electronegative and hydrogen bond-accepting groups that could strengthen their interaction with amide bond motif in POx micelle. This specific interaction between PTX and POx could increase the colloidal stability even when PLX3397 is additionally encapsulated [33,35]. In any case, the best strategy for these micellar formulations of the drugs is to keep them in the dry lyophilized form with rehydration prior to the use (Supplementary Fig. S1).

The drug release profiles were examined under sink conditions. The single drug POx-PTX micelles showed sustained drug release, with 50% drug released at 5 h (Fig. 1**(c)**). The single drug POx-PLX micelles also showed similar sustained drug release profile; however, precipitation was observed after 5 h. POx-PTX/PLX remained stable during entire observation time. The release of each drug from the co-formulated POx-PTX/PLX micelles was slower than that from

(a)

Anticancer agent (PTX) and CSF1R inhibitor (PLX3397)						
Feeding ratio (g/L) POx/PTX/PLX3397	LE (%)		LC (%)		D_{eff} (nm)	PDI
	PTX	PLX3397	PTX	PLX3397		
10/8/0	95.9 ± 2.1	-	43.4 ± 0.5	-	34.6 ± 0.7	0.11 ± 0.02
10/4/1	90.9 ± 6.2	95.5 ± 23.4	24.9 ± 1.0	6.5 ± 1.4	40.4 ± 5.8	0.16 ± 0.02
10/4/2	93.4 ± 3.7	93.7 ± 9.4	23.9 ± 0.4	12.0 ± 0.9	51.3 ± 5.2	0.17 ± 0.02
10/4/4	94.0 ± 3.9	99.9 ± 9.3	27.3 ± 0.8	28.5 ± 1.9	57.0 ± 8.2	0.16 ± 0.02
10/2/4	98.8 ± 7.5	98.2 ± 2.4	12.4 ± 0.9	24.7 ± 0.7	42.9 ± 7.1	0.16 ± 0.01
10/1/4	96.5 ± 10.0	92.1 ± 5.7	6.6 ± 0.7	25.1 ± 1.2	42.5 ± 3.5	0.18 ± 0.02
10/0/8	-	98.8 ± 6.1	-	44.1 ± 1.5	37.9 ± 1.2	0.05 ± 0.02

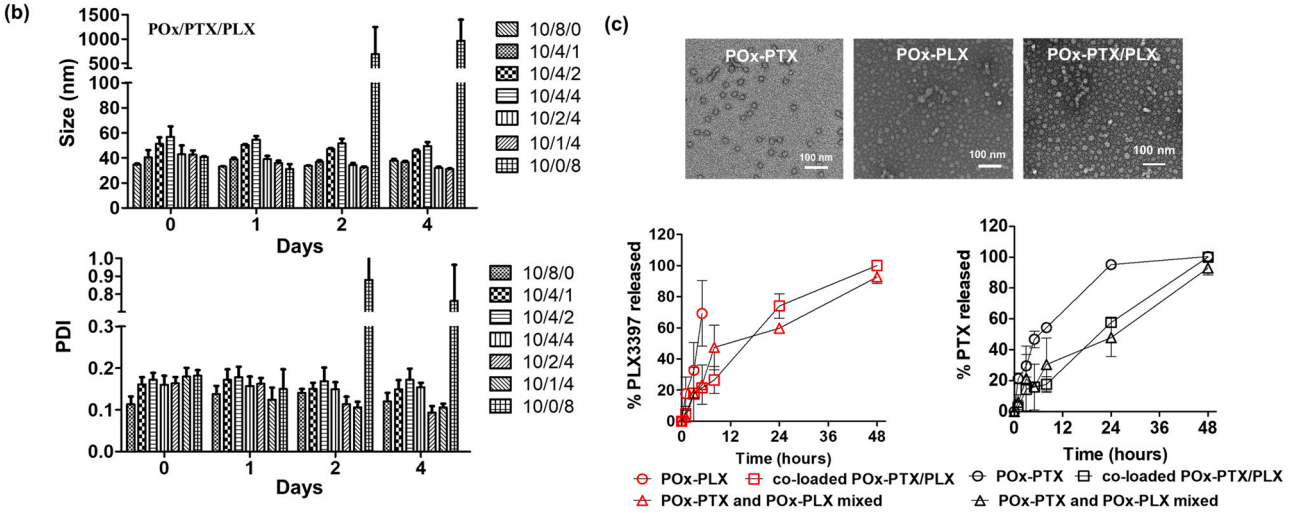

Fig. 1. Physicochemical properties of drug-loaded micelles. (a) drug loading (expressed as loading efficiency (LE) (%) and loading capacity (LC) (%)) and size distribution (expressed as D_{eff} and polydispersity index (PDI)) of drug-loaded micelles. (LE (%) = M_{drug} / $M_{drug\ added}$ × 100 (%) and LC (%) = M_{drug} / (M_{drug} + $M_{excipient}$) × 100 (%)) (b) stability of drug-loaded micelles in solution as assessed by particle size and PDI over time measured by dynamic light scattering (DLS). (c) particle morphology by transmission electron microscopy (TEM) and drug release profiles (left: PLX3397 and right: PTX) from single drug micelles (POx-PLX or POx-PTX), co-loaded POx-PTX/PLX, or POx-PLX and POx-PTX mixed prior to the release test. All measurements were done in triplicate and values are average of three replications with standard deviation except for TEM image.

the single drug micelles, which could be attributed to attractive drug-drug/drug-polymer interactions in these complex mixtures [28,29,36]. Notably, when the single drug micelles were pre-mixed in the same proportion their release profiles measured few minutes after mixing were practically the same as that of POx-PTX/PLX (Fig. 1**(c)**). This can be explained by inter-micellar drug exchange resulting in reconstitution of the co-loaded system.

Drug combination micelles exhibit synergy in breast cancer cells

While the main objective of this study using PLX3397 was to deplete the macrophage population in TME to treat TNBC tumors, we point out that PLX3397 is also known as an inhibitor of c-Kit, a receptor tyrosine kinase, with half-maximal inhibitory concentration (IC_{50}) of 10 nM [37,38]. Therefore, this drug can elicit direct anticancer effect by inhibiting proliferation of tumor cells via the c-Kit pathway, as was observed in many tumor models [39,40]. Thus, we evaluated the cytotoxicity of the single and combination drug micelles in vitro, using 4T1, T11-apobec and T12 TNBC mouse cell lines derived from the respective transplantable tumors. (Fig. 2 **(a)** and **(b)**). In the 4T1 cell line, the IC_{50} values of POx-PTX and POx-PLX were 25.9 μg/ml and 151.3 μg/ml, respectively. However, the POx-PTX/PLX displayed much lower IC_{50} values (for instance, 0.72 μg/ml of total drug at 1:1 mass ratio), suggesting strong synergistic effect between the drugs. A similar phenomenon was seen in the two other TNBC cell lines. For example, in T11-apobec the IC_{50} value for drug combination at 1:1 mass ratio was 0.02 μg/ml compared to 0.09 μg/ml and 1.06 μg/ml for POx-PTX and POx-PLX, respectively. Therefore, we determined the combination indices (CI) of the PTX and PLX3397 in these cell models as defined by Chou and Talalay [41]. Very strong synergy between the drugs (CI < < 1) was observed in 4T1 and T11-apobec cells for nearly the entire range of the cell fraction affected (Fa) (Fig. 2**(b)**). In the T12 cells there was some antagonism at Fa < 0.3 but overall, the drugs also displayed strong synergy at Fa > 0.3. In this cell line the IC_{50} value for the drug combination was still much lower than for the single drug micelles (0.09 μg/ml for the combination at 1:1 drug ratio vs. 0.33 μg/ml for POx-PTX, and 0.76 μg/ml for POx-PLX). Interestingly, drug synergy was exhibited at various PTX: PLX3397 drug mass ratios ranging from 4:1–1:4 as demonstrated using the 4T1 cell model. Since we observed synergy regardless of the drug ratio in 4T1 cells, we selected one ratio for the two other cell lines. The combination drug micelles also induced apoptosis and necrosis to a greater extent in the TNBC cells (at equivalent drug concentration 1 μg/ml) as determined after 24-h exposure (Fig. 2**(c)**). Overall, in the studied breast cancer models, the drug combinations were substantially more active than either of the single drugs. Based on this in vitro analysis, we fixed the POx to drug mass ratios at 10/4 for single drug micelles or 10/4/4 for POx-PTX/PLX micelles and proceeded to in vivo evaluation.

Anti-tumor effects in TBNC models

Next, we explored the antitumor activity of our agents in immune-competent orthotopic environment using the same three models tested above, namely: (1) 4T1, (2) T11-apobec, and (3) T12 (Fig. 3**(a-c)**). 4T1 is an aggressive tumor model that spontaneously

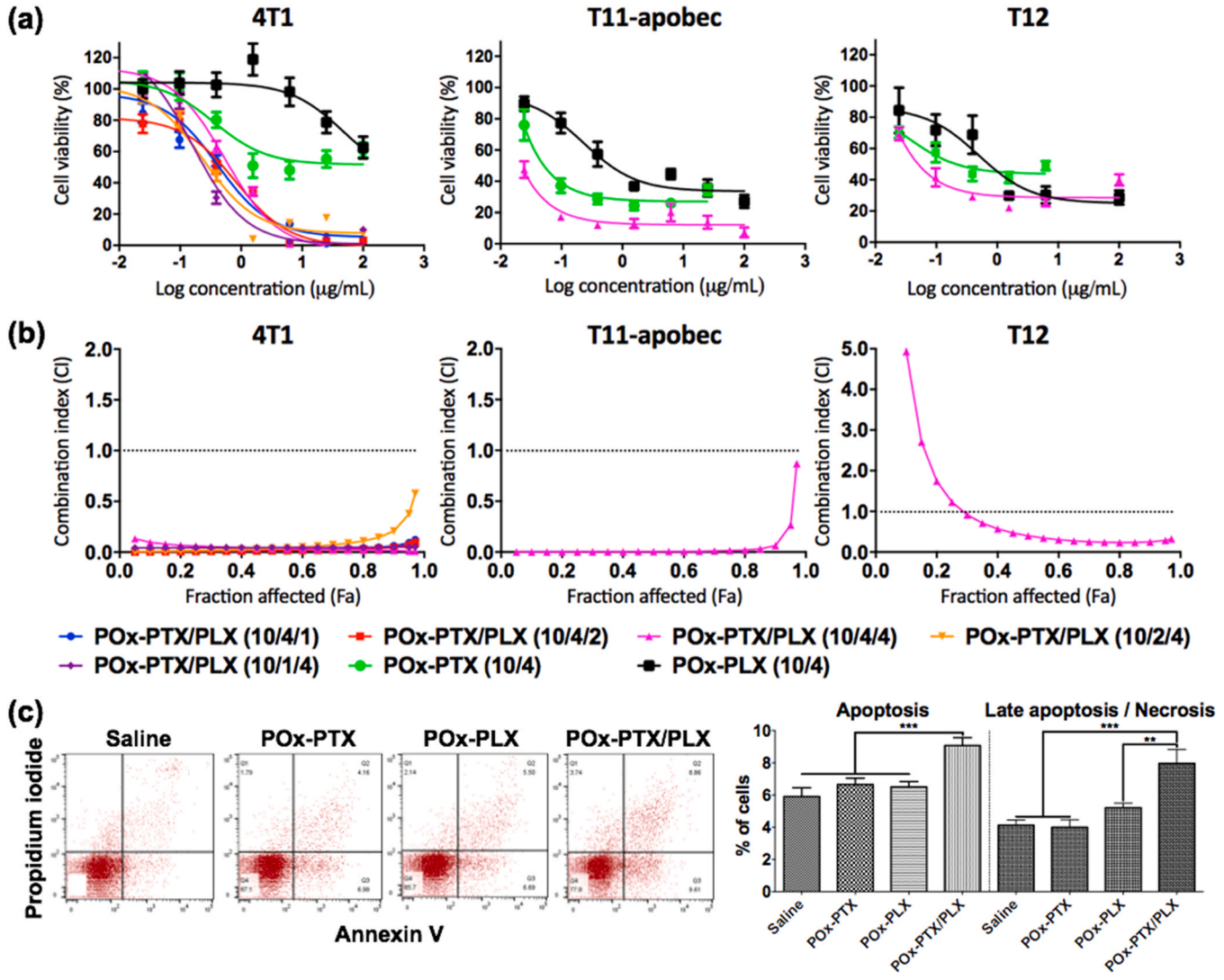

Fig. 2. in vitro evaluation. (a) Cytotoxicity and (b) Combination index of drug-loaded micelles in the 4T1, T11-apobec and T12 cell lines. (a) Ordinate presents the logarithmic scales of the concentrations of the respective single drugs in POx-PTX or POx-PLX, or PTX in POx-PTX/PLX. (a, b) The numbers in the brackets designate the mass ratios POx: PTX (10/4) or POx: PLX3397 (10/4) for the single drug micelles, or POx: PTX: PLX3397 (10/4/1; 10/4/2; 10/2/4; 10/1/4) for the co-loaded micelles. (c) Flow cytometry analysis of apoptosis and necrosis using annexin V and propidium iodide double staining in 4T1 cells treated by saline, POx-PTX (10/4), POx-PLX (10/4) or (POx-PTX/PLX (10/4/4) at PTX and/or PLX3397 = 1 μg/ml. Statistical comparison was done using a one-way analysis of variance (ANOVA) and followed by Bonferroni post-tests for multiple comparison (n = 4–5). Statistical difference: $^{*}p < 0.05$, $^{**}p < 0.01$, $^{***}p < 0.001$.

metastasize to the lungs, liver, lymph nodes, and brain [42] and is resistant to αPD-L1 therapy [43] but sensitive to radiation and chemotherapy [44,45]. The two other tumors are derived from TP53-/- genetically engineered mouse models (GEMMs) that have shown genomic and genetic similarities to human TNBCs [46–48]. T11-apobec tumors are deficient in P53, overexpressing APOBEC3 to increase the tumor mutational burden (TMB), and closely recapitulate the genetic lesions and immune responses found in patients with claudin-low breast cancer [49]. The T12 tumor model is another closely related TNBC claudin-low model that has high level of expression of CSF1R and markers related to immunosuppressive TAMs [50]. It has previously shown a partial response to oral PLX3397 [50]. Prior to mouse treatment experiments, we analyzed drug toxicity in various formulations to ensure that the doses and regimens used were safe (Supplementary Fig. S2). In our previous PK studies of POx-PTX in tumor-bearing mouse models, we found that it took more than 48 h for the drug to be eliminated from the blood and the tumor [51]. Therefore, we set the drug administration interval to at least three days. Additionally, when the samples were injected four times over two weeks, there was no significant change in body weight, but increasing the injections to six times over three weeks resulted in a significant decrease in body weight (Supplementary Fig. S2). As a result, we decided to administer the samples q4d regimen for two weeks.

4T1 orthotopic model of TNBC. The tumor growth curves are presented in Fig. 3**(a)**. In the saline control group, the tumor volume increased from ca. 100 to ca. 2000 mm^3 over 20 days. In this TNBC model, neither POx-PLX (75 mg/kg) nor POx-PTX (30 mg/kg) slowed down the tumor growth. The groups treated with the high-dose POx-PTX (75 mg/kg) displayed significant tumor inhibition effects compared to the saline control or POx-PTX (30 mg/kg). The co-loaded POx-PTX/PLX produced the most pronounced antitumor effect that was also dose-dependent (Fig. 3**(a)**, and supplementary Fig. S3). The treatment with the higher dose POx-PTX/PLX (75 mg/kg PTX and 75 mg/kg PLX3397) was superior to all other treatments including POx-PTX (75 mg/kg). The POx-PTX/PLX at this dose also showed superiority vs. the combination treatment with the maximum tolerated dose (MTD) of PTX and PLX3397 in the standard Cremophor EL vehicle (Supplementary Fig. S3 and Table S2) and increased apoptosis in the tumor tissue (Supplementary Fig. S4).

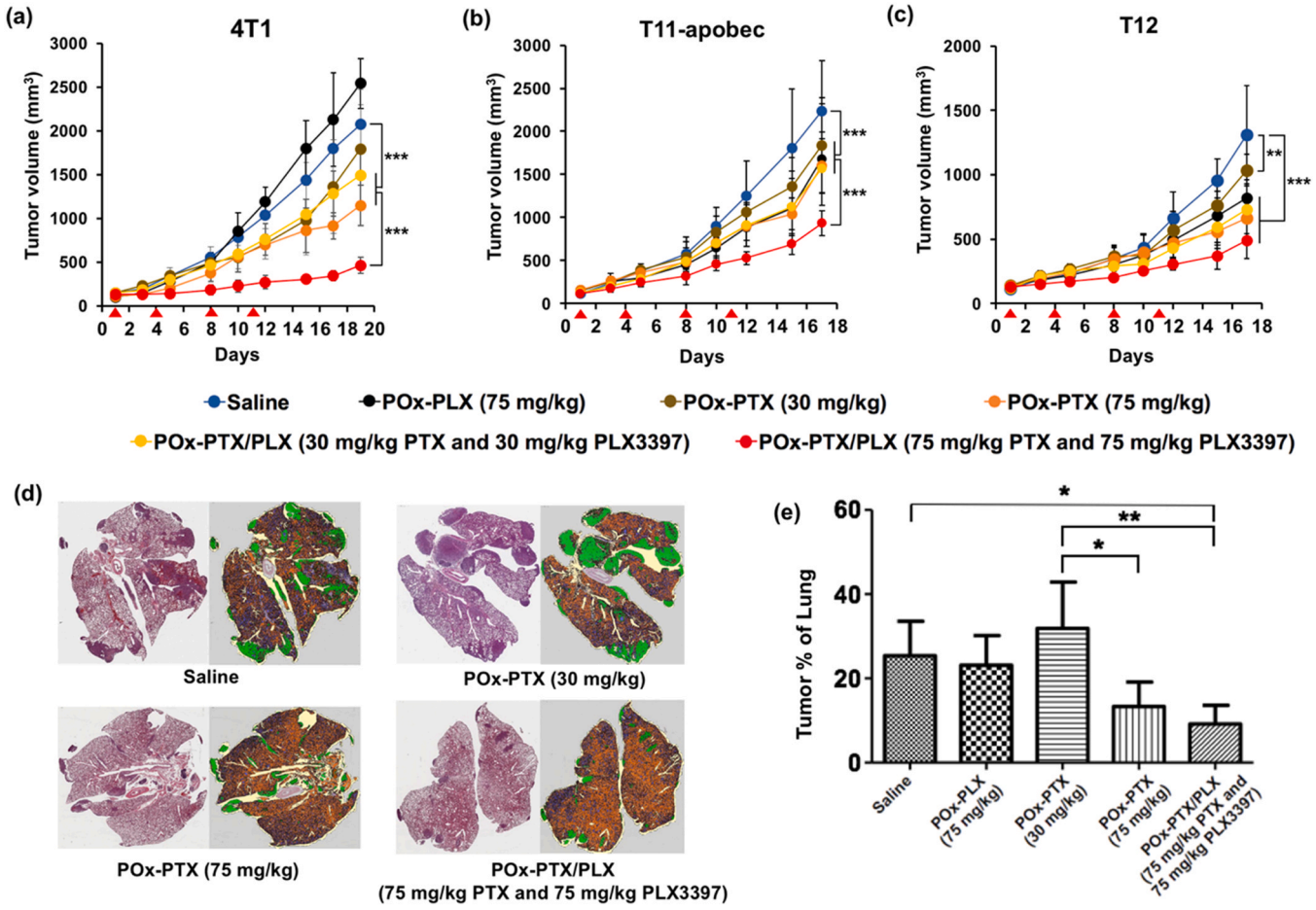

Fig. 3. (a-c) Primary tumor inhibition and (d, e) suppression of lung metastases in mice bearing orthotopic TNBC tumors (a, d, e) 4T1 (b) T11-apobec (c) T12 (a-c). The animals (n = 4–8) were injected iv (as shown by arrows, q4d × 4) with: saline, POx-PLX (75 mg/kg), POx-PTX (30 mg/kg), POx-PTX (75 mg/kg), POx-PTX/PLX (30 mg/kg PTX and 30 mg/kg PLX3397) and POx-PTX/PLX (75 mg/kg PTX and 75 mg/kg PLX3397). (d) Representative H&E and overlay images of lungs from mice with 4T11 tumors harvested between 24 days, and (e) quantification of lung metastasis following indicated treatments. Statistical comparisons (a-c) for tumor inhibition were done using two-way ANOVA, followed by Bonferroni post-test (n = 4–5) and (d) for lung metastases by one-way ANOVA with Tukey's test. Statistical difference: * ($p < 0.05$), ** ($p < 0.01$), and *** ($p < 0.001$). See supplementary Table S1 for the complete statistical comparison between all groups for primary tumors (a-c).

Along with the effect on the primary tumor, both the high-dose POx-PTX and POx-PTX/PLX significantly decreased the levels of metastases in lung tissues compared to the POx-PLX, lower dose POx-PTX (30 mg/kg), and the saline control (Fig. 3**(d) and (e)**). A promising approach for treating breast tumors in a clinical setting is a combination of immune checkpoint inhibitors and nab-paclitaxel. In this context, we evaluated the combination of a mouse antibody against programmed cell death protein 1 (PD1), anti-PD1 and POx-PTX/PLX in 4T1 model. In our experiment, however, the combination of anti-PD1 and POx-PTX/PLX did not provide any discernible benefit over POx-PTX/PLX therapy either in primary tumor inhibition nor in suppressing the metastatic spread (Supplementary Fig. S5**(a-c)**).

T11-apobec orthotopic model of TNBC. The combination treatment with POx-PTX/PLX (75 mg/kg PTX and 75 mg/kg PLX3397) also showed significant anti-tumor effect in the orthotopic T11-apobec model compared to the saline or other treatment groups (Fig. 3**(b)**). The antitumor effects of single drugs or drug combination at the lower dose were significant compared to the saline control but small and indistinguishable from each other. (Fig. 3**(b)**).

T12 orthotopic model of TNBC. In this model, each single drug-loaded POx micelle treatment caused modest tumor inhibition. As observed in the previous models, the POx-PTX/PLX (75 mg/kg PTX and 75 mg/kg PLX3397) exhibited the most pronounced antitumor effect, but differences were not statistically significant compared to POx-PTX (75 mg/kg) (Fig. 3**(c)**).

Gene expression analysis of mammary tumors of mouse models

While various factors determine drug sensitivity, the molecular subclassification of breast cancer may offer important insight to drug response. Therefore, in addition to the three models used in this study, we utilized gene expression analysis on a total of 232 mice, representing 29 mammary tumor models, most of which come from Hollern et al. [52], to learn about the expression phenotypes of these three tested models. Based on the genomic expression characteristics presented in Fig. 4, the T11-apobec and T12 tumors clearly display the Claudin-low gene expression phenotype, characterized by low expression of many cell-cell adhesion proteins including multiple claudin proteins, EpCAM and CDH1. Furthermore, the 4T1 model displays an intermediate gene expression pattern that lacks clear Claudin-low or basal-like transcriptomic features, which is contrary to previous literature that suggests this model is basal-like [53–55]. Based on the gene expression analysis of this study, it can be postulated that the T11-Apobec and T12 tumor models are less sensitive to POx-PTX/PLX combination therapy compared to 4T1 due to their differences in molecular subtype; T11-Apobec and T12 belong to the Claudin-low subtype, which is known to be highly aggressive and exhibits poorer prognosis characteristics in comparison to other subtypes [56–58].

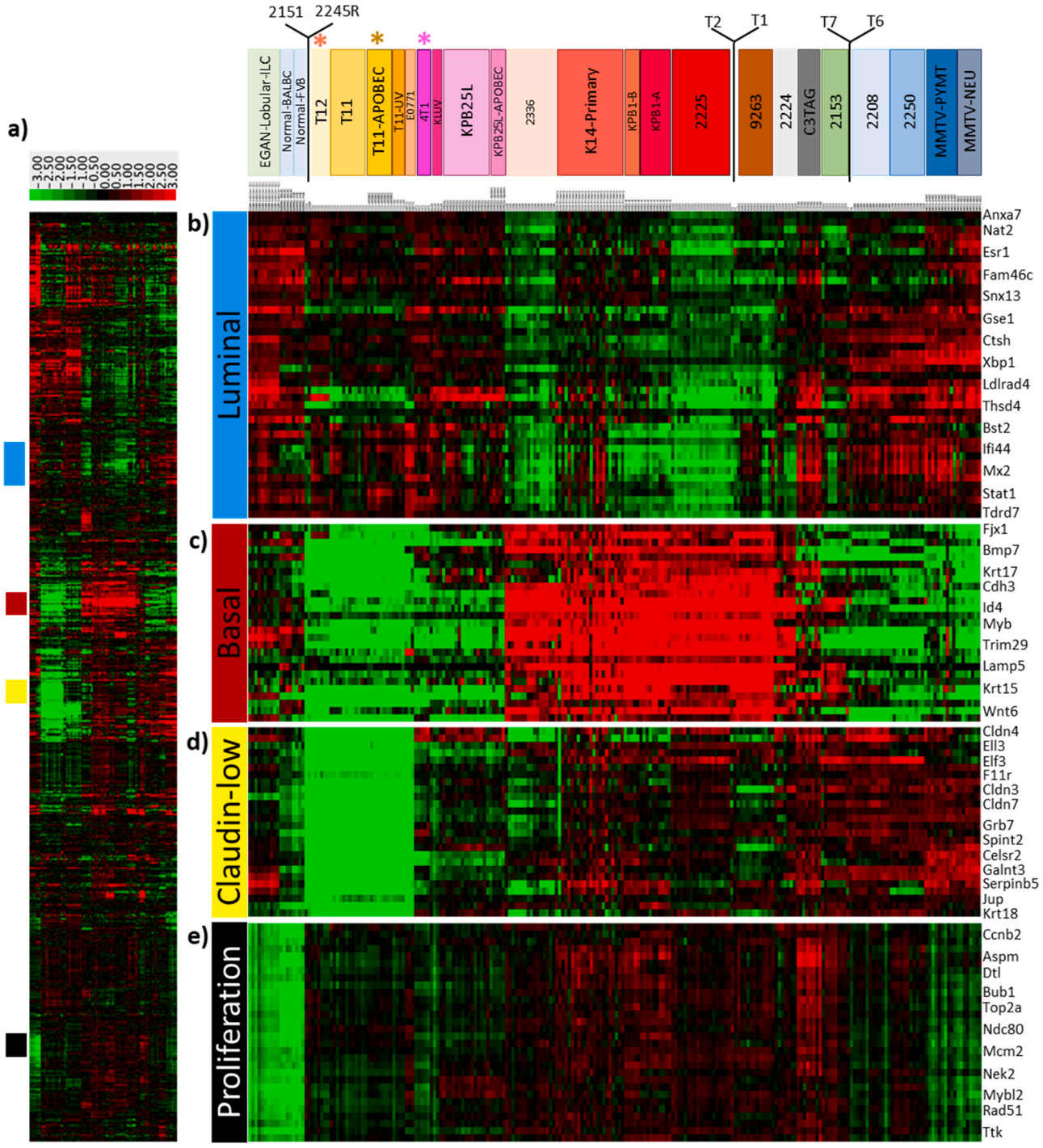

Fig. 4. Intrinsic gene set cluster analysis of mouse tumor models. **(a)** Overview of the entire cluster based on the RNA expression of 1723 intrinsic genes for 232 individual mouse mammary tumors and normal mammary gland controls, covering 31 models (marked in different colors over the columns in the center panel). **(b)** Luminal epithelial expression subcluster. **(c)** Basal gene expression subcluster. **(d)** Claudin-low subcluster, with low expression of Claudins 3, 4, and 7. Both T11-APOBEC (yellow star), and T12 (orange star) show low expression for this subcluster, while 4T1 shows average expression (pink star). **(e)** Proliferation subcluster indicating highest expression among basal-like tumor models.

Effect of drug co-formulation vs. separate administration

We further explored whether there is a benefit in co-loading PTX and PLX3397 into a single micellar vehicle vs. administering them separately (Fig. 5**(a)**). We compared two drugs in one micelle, POx-PTX/PLX, with the same drugs loaded in separate micelles and mixed immediately before injection or administered sequentially. Since PLX3397 is orally available [40], we also explored the combination treatment with POx-PTX micelles injected iv and free PLX3397 given by oral gavage in a standard vehicle (5% DMSO, 45% PEG300, and 5% Tween 80 in distilled water) using previously described dose regimen [59]. As a reference point, we also included a group treated with POx-PTX. The results of this experiment suggest a clear benefit of co-loaded drug micelles compared to separate treatments (Fig. 5**(b)**). Although the combination treatment with POX-PTX iv and PLX3397 orally showed some improvement over single POx-PTX, this combination was much less effective compared to POx-PTX/PLX at the same cumulative dose. Likewise, the sequential iv

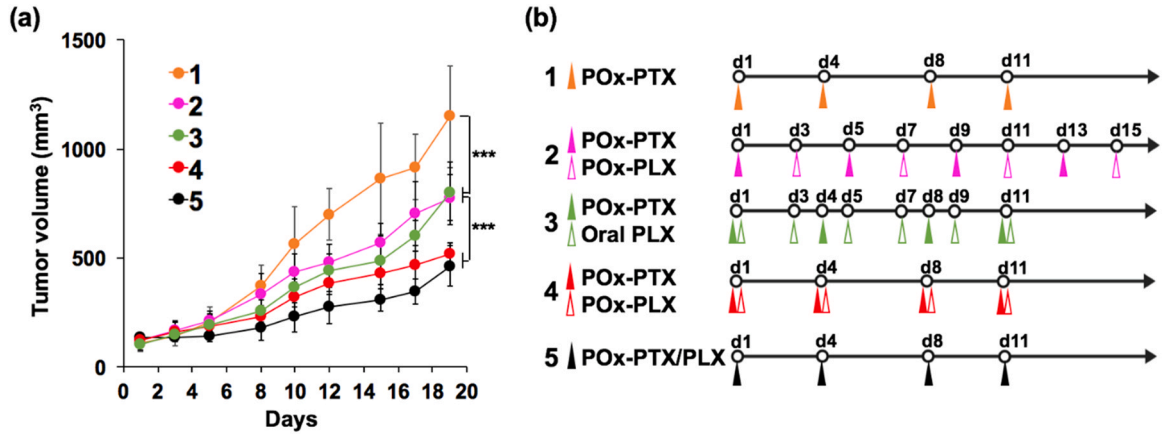

Fig. 5. Dependence of anti-tumor effects of the PTX and PLX3397 combination therapy on the drug formulation, dose regimen and administration route in mice with orthotopic TNBC 4T1 tumors. (**a**) Antitumor effects in animals with tumors treated as schematically shown in (**b**) with 1 – POx-PTX (75 mg/kg), 2 – sequentially injected POx-PTX (75 mg/kg) and POx-PLX (75 mg/kg), 3 – POx-PTX (75 mg/kg) and oral PLX3397 (50 mg/kg) in standard vehicle, 4 – POx-PTX (75 mg/kg) and POx-PLX (75 mg/kg) mixed immediately prior to injection (simultaneous), 5 – co-loaded POx-PTX/PLX (75 mg/kg PTX and 75 mg/kg PLX3397). All treatment groups received drugs iv except for 3 where the micellar POx-PTX was injected iv and PLX3397 was administered orally. The 1 and 2 datasets are same as in Fig. 3(**a**). Statistical comparison of data for tumor inhibition was done using a two-way ANOVA and followed by Bonferroni post-tests for multiple comparisons (n = 4–5). Statistical difference: * ** $p < 0.001$. See supplementary Table S3 for the complete statistical comparison between all groups.

administration of POx-PTX and POx-PLX was more active than POx-PTX, but less active than co-loaded POx-PTX/PLX. The separate micellar drugs mixed prior to injection have shown similar activity to that of POx-PTX/PLX, which could be explained by the rapid inter-micellar drug exchange resulting in reconstitution of the co-loaded system [28,29,36].

Assessment of activation of immune cells population in TME

To uncover the effects of our treatments on the TME we harvested in vivo tumors and performed immune phenotyping by multi-panel parameter flow cytometry (Fig. 6, and supplementary Fig. S6, Table S4**,** and **S5**). To analyze the changes in immune cells, we selected a specific time point where the in vivo responses are most pronounced, and the changes are substantial enough to enable a comparison of all groups. After the fourth drug injection, the overall cell viability within the tumor was too low due to factors such as necrosis, making it less ideal to compare the immune cell population between sample treated groups. In contrast, three days after the second dose, more than 30% of the cells were still alive, so we chose this time point as the analysis point for the immune cell population. In the 4T1 model, flow cytometry showed that $CD8^+$ T cells and $CD4^+$ T cells were markedly increased in all PTX containing treatment groups compared to control or PLX3397 treated groups, while there were no statistical differences between the low and high dose POx-PTX and/or POx-PTX/PLX treated groups. In the T12 orthotopic model, similar trends were observed for $CD8^+$ T cells and $CD4^+$ T cells, but differences were not statistically significant in the group comparisons (1-way ANOVA with Turkey post-test, see Supplementary Table S6). In the T11-apobec model, the POx-drug formulation treatment did not change the $CD8^+$ populations compared to the control group, but $CD4^+$ were decreased by the POx-PTX/PLX treatment. There were no statistical changes in T_{regs} population after the treatments compared to control groups in any of the three tumor models.

We also assessed the MDSC subpopulations (Fig. 6). In 4T1 or T11-apobec models, POx-PLX had no effect on granulocytic MDSC (G-MDSC) or monocytic MDSC (M-MDSC). Interestingly, in the T12 model, POx-PLX increased both M-MDSC and G-MDSC subpopulations, while POx-PTX and POx-PTX/PLX depleted these subpopulations. Both POx-PTX and POx-PTX/PLX depleted G-MDSC and produced no changes on M-MDSC in 4T1 or T11-apobec tumors. Statistical analysis showed a trend or significant difference in G-MDSC between POx-PTX (30 mg/kg) > POx-PTX (75 mg/kg) > POx-PTX/PLX groups (see Supplementary Table S6).

Finally, we assessed TAMs (Fig. 7). As expected, POx-PLX decreased the total TAMs in all three tumor models. Interestingly, this drug enhanced the M1-like macrophages in 4T1 and T11-apobec but not in T12 tumors, while M2-like macrophages were not changed in any of these tumors. The difference in response may be due to the enrichment of T12 tumors with M1-like macrophages [50]. However, in all models POx-PLX decreased the M2/M1 ratios suggesting pro-inflammatory repolarization of the TAMs. Interestingly, POx-PTX also appeared to decrease the M2/M1 ratio, at least in the case of 4T1 tumors (see Supplementary Table S6 for analysis of significance). The POx-PTX/PLX combination decreased the M2/M1 ratios compared to controls in all cases.

Effect of immune cell depletion on the anti-tumor activity of drug combinations

To assess the potential role of T cell-mediated anti-tumor immunity, we determined whether the depletion of the $CD4^+$ and $CD8^+$ T cells can interfere with the therapeutic effects of our drugs on tumor growth and lung metastases (Fig. 8 and supplementary Fig. S7). We used commercial antibodies against CD4 + or CD8 + and treatment regimens previously shown to deplete these T cell populations in 4T1 in BALB/c mice [60–63]. The antibody injections do not seem to influence the tumor growth curves in the saline control, and POx-PTX (30 mg/kg) or POx-PTX (75 mg/kg) treatment groups (Fig. 8(**a–c**)). The effects on lung metastases in these groups were also insignificant, except for the control group, where the depletion of $CD8^+$ T cells increased metastatic lesions. However, in animals treated with POx-PTX/PLX, the depletion of either $CD4^+$ or $CD8^+$ T cells significantly increased both the tumor growth rates and the metastatic lesions ((Fig. 8(**d**)). Overall, these data indicate that the effects of POx-PTX/PLX on primary tumor growth and lung metastases are $CD4^+$ and $CD8^+$ cell-dependent.

Effect of the treatments of the tumor rechallenge and induction of ICD

To further demonstrate the involvement of the immune component in the anti-tumor responses to our drugs, we carried out the vaccination-rechallenge experiment in vivo [64]. For this

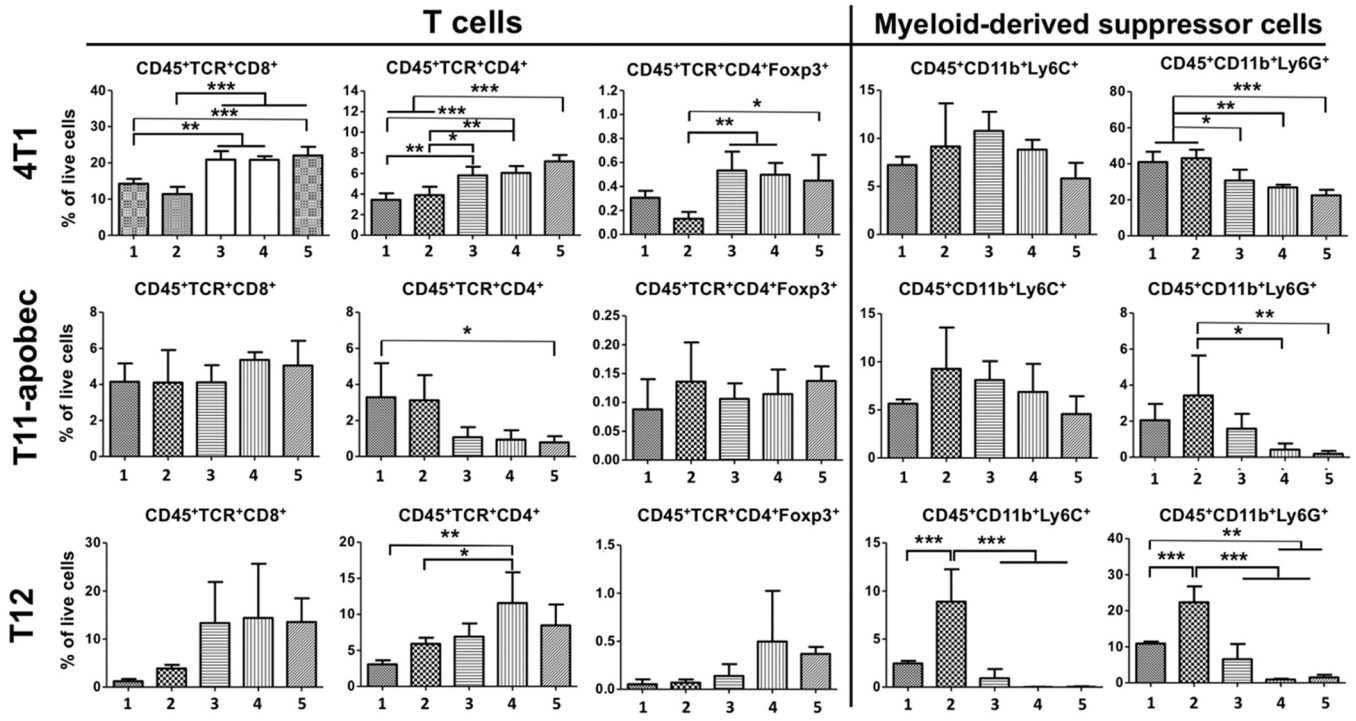

Fig. 6. Immune phenotyping to demonstrate the effect of drug formulations on TNBC tumor models. The animals received saline or drug-loaded micelles iv using q4d × 2 with 1 – normal saline, 2 –POx-PLX (75 mg/kg), 3 – POx-PTX (30 mg/kg), 4 – POx-PTX (75 mg/kg), and 5 – co-loaded POx-PTX/PLX (75 mg/kg PTX and 75 mg/kg PLX3397). 3 Days after 2nd dose of treatment, tumors were harvested to perform flow cytometry to show the impact on $CD8^+$ T cells, $CD4^+$ T cells, T_{reg}, M-MDSCs and G-MDSCs. Statistical comparison of data for tumor inhibition was done using a one-way ANOVA with Tukey's test for multiple comparisons (* ($p < 0.05$), ** ($p < 0.01$), and *** ($p < 0.001$)). (see Supplementary Table S6 for statistical comparisons between all groups).

experiment, an orthotopic 4T1 tumor model was established by subcutaneously injecting 1×10^6 4T1 tumor cells into the right 4th mammary fat pad. The primary tumor bearing mice received saline or drug treatments by iv injection at days −6 and −3, and the secondary 1×10^6 4T1 cells were inoculated into the left 4th mammary fat pad at day 0 (Fig. 9**(a)**). The secondary tumor growth effects were monitored for 14 days (Fig. 9**(b)**). Notably, when the dosing amount of PTX during treatment of the primary tumor increased to 75 mg/kg, significant suppression of the secondary tumor growth was observed compared to saline and lower PTX dose of 30 mg/kg. The treatments using the combination drug micelles revealed a trend for further suppression of the secondary tumor, although in this case, the difference with the single high dose POx-PTX micelles was insignificant. Based on the previously reported pharmacokinetics of POx-PTX micelles [65] at 72 h post injection the amount of drug remaining in the plasma (and tissue) is less than 0.1 μg/ml (or gram of tissue). This amount remaining after treatment of the primary tumor could not cause anti-tumor activity against the tumor challenge (IC_{50} in 4T1 is approximately 2.4 μg/ml). However, to address this point a separate tumor growth study was conducted as presented in supplementary Fig. S8. In this experiment, the tumor-free animals were treated with two doses of the drug and then the "secondary" tumor was inoculated 3 days after the last dose of drug like in the previous experiment. There was no difference in the tumor growth rate between saline and drug treated groups. Therefore, the decrease in the secondary tumor growth observed in the vaccination-rechallenge experiment is likely due to the induction of the immunological memory because of the response elicited by the drug treatment of the primary tumor. Several studies indicated that PTX can induce ICD in TNBC and other tumors [66–68]. Therefore, we examined whether the PTX in polymeric micelles can induce ICD in 4T1 cells by measuring extracellular ATP and the surface expressions of CRT as danger-associated molecular patterns (DAMPs) associated markers [69]. As the drug dose increased, the release of ATP and expression of CRT gradually increased (Supplementary Fig. S9). To further identify the ICD, the primary tumor after the second drug treatment was harvested, sectioned, and stained for CRT and HMGB1. Both markers were increased, especially in the high-dose PTX and combination drug treatments suggesting that these treatments induce ICD in the tumors (Fig. 9**(c)**).

Discussion

The use of nanotechnology approaches for the delivery of biologically active molecules has revolutionized human health as most obviously seen from the advent and implementation of RNA vaccines during the coronavirus infection pandemic [70,71]. POx micelle nano-assemblies is a new platform technology showing extremely high entrapment of small molecules with minimal polymeric excipient [36]. Prior studies have shown that this technology enables 1) the delivery of high-dose PTX with less toxicity than conventional paclitaxel [65], and 2) the co-deliver of two drugs in a single micelle with increased tumor distribution of both drugs [28,29]. Both these effects were shown to increase anti-cancer therapy outcomes across diverse cancers in rodent models.

Here, for the first time, we demonstrate that high-dose chemotherapy of PTX in POx micelles potentiates the immunological effects of the drug therapy in three immune-competent mouse models of TNBC. In this study, with POx-PTX, we observe enhanced tumor growth inhibition and suppression of lung metastases along with the changes in TME, including increased levels of $CD4^+$ and $CD8^+$ T cells (in two out of three tumor models), suppression of MDSC (G-MDSC), and, notably, repolarization of TAMs toward M1-like pro-inflammatory phenotype. Moreover, POx-PTX treatment at the highest dose used (75 mg/kg) (which is still twice less than the reported MTD [65]) establishes long-term immune memory against tumor cells challenge. Notably, PTX was previously shown to induce ICD, a form of regulated cell death that triggers adaptive immunity

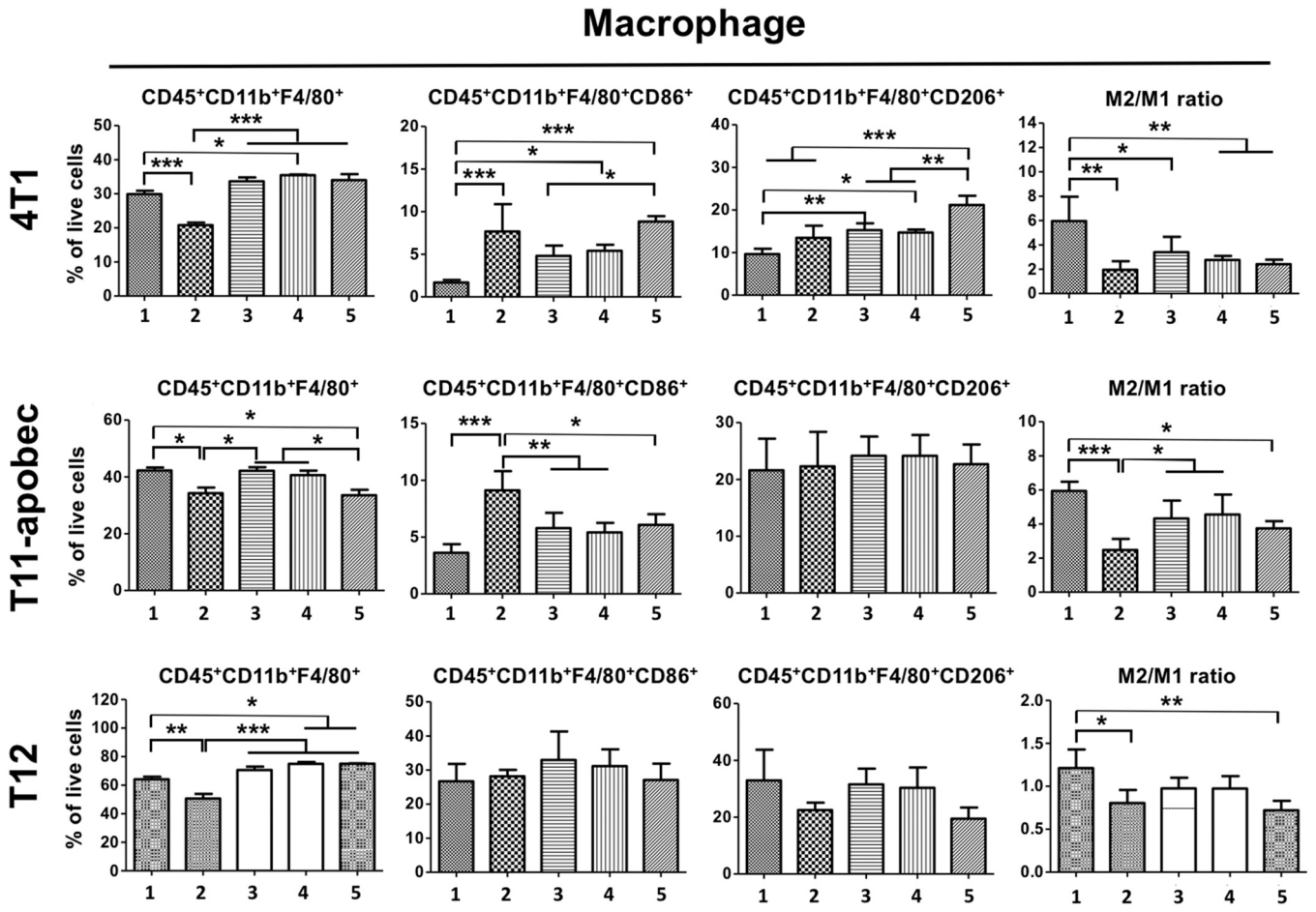

Fig. 7. Immune phenotyping to demonstrate the effect of drug formulations on TNBC tumor models. The animals received saline or drug-loaded micelles iv using q4d × 2 with 1 – normal saline, 2 –POx-PLX (75 mg/kg), 3 – POx-PTX (30 mg/kg), 4 – POx-PTX (75 mg/kg), and 5 – co-loaded POx-PTX/PLX (75 mg/kg PTX and 75 mg/kg PLX3397). 3 Days after 2nd dose of treatment, tumors were harvested to perform flow cytometry to show the impact on total macrophages ($CD45^+CD11b^+F4/80^+$), M1-like macrophages ($CD45^+CD11b^+F4/80^+CD86^+$), M2-like macrophages ($CD45^+CD11b^+F4/80^+CD206^+$), and M2/M1 ratios. Statistical comparison of data for tumor inhibition was done using a one-way analysis of variance (ANOVA) with Tukey's test for multiple comparisons (* ($p < 0.05$), * * ($p < 0.01$), and * ** ($p < 0.001$)). (see Supplementary Table S6 for statistical comparisons between all groups).

through production of neoantigens and release of DAMPs [66–68]. PTX also can alter TAMs toward a pro-inflammatory phenotype and produce an anti-tumor effect by activating Toll-like receptor 4 [72]. In clinical settings, the need for steroid premedication to decrease the adverse effects of conventional paclitaxel may blur the anti-cancer immune responses [73]. Here, due to the reformulation of PTX in POx micelles, we could administer high-dose PTX therapy and indeed observe the dose-dependent ICD induction in the TNBC model. Notably, the greatest ICD activation in tumors, as assessed by the expression of the DAMPs associated markers, was seen at the highest POx-PTX dose (75 mg/kg), which is not achievable with conventional paclitaxel (MTD 20 mg/kg with q4d × 4 regimen [65]. The ICD induction and indications of the enhanced anti-tumor immunity provide new, additional, and important evidence of a potential benefit of POx micelle system that enhances the PTX effect on the target by delivering high dose with minimal formulation toxicity [65]. The PTX POx micelle formulation does not induce complement activation [65,74], which may abolish the future need for premedication in clinical use.

For the combination of chemo- and immunotherapy, we have chosen a small molecule inhibitor of CSF-1R, PLX3397 (Pexidartinib). Pexidartinib was initially developed by Plexxikon Inc. and Daichi-Sankyo, and advanced to a multi-center international clinical trial [75]. With positive clinical outcomes for patients with symptomatic tenosynovial giant cell tumors, PLX3397 received regulatory approval in 2019 as TURALIO® in United States [75]. Although this agent has been administered orally in the clinic, we assessed whether its co-formulation with PTX in polymeric micelles could be advantageous for systemic administration compared to oral dosing. Indeed, we observed an improved anti-tumor effect of PTX and PLX3397 co-formulated in POx micelles and administered iv compared to the same cumulative dose of both drugs with POx-PTX injected iv and PLX3397 dosed orally in a standard vehicle. Previously, DeNardo et el. reported improved antitumor activity of iv PTX (via into the retroorbital plexus) and oral PLX3397 combination in treating MMTV-PyMT TNBC [22]. However, this murine tumor model was quite sensitive to the low-dose PTX therapy (10 mg/kg, q5d ×3 or q5d × 4). In contrast, all our TNBC models have shown little or no response to PTX at 30 mg/kg (q4d × 4). Across all tumor models used in this study, the co-formulated POx-PTX/PLX was more potent than the single drug treatments. Interestingly, nearly the same improved anti-tumor effect was observed with the two micellar drugs mixed before injection, which may be a technological advantage for future drug development due to ease of manufacturing and application in some clinical settings. Prior studies of chemotherapeutic agents in POx micelles, such as PTX and cisplatin prodrug derivative, suggested that these agents were more active in co-formulation [28]. Here, we observed a similar effect for combining chemotherapeutic and immunotherapeutic agents. Notably, PLX3397 has a direct cytotoxic effect via inhibiting c-kit and fms-like tyrosine kinase 3

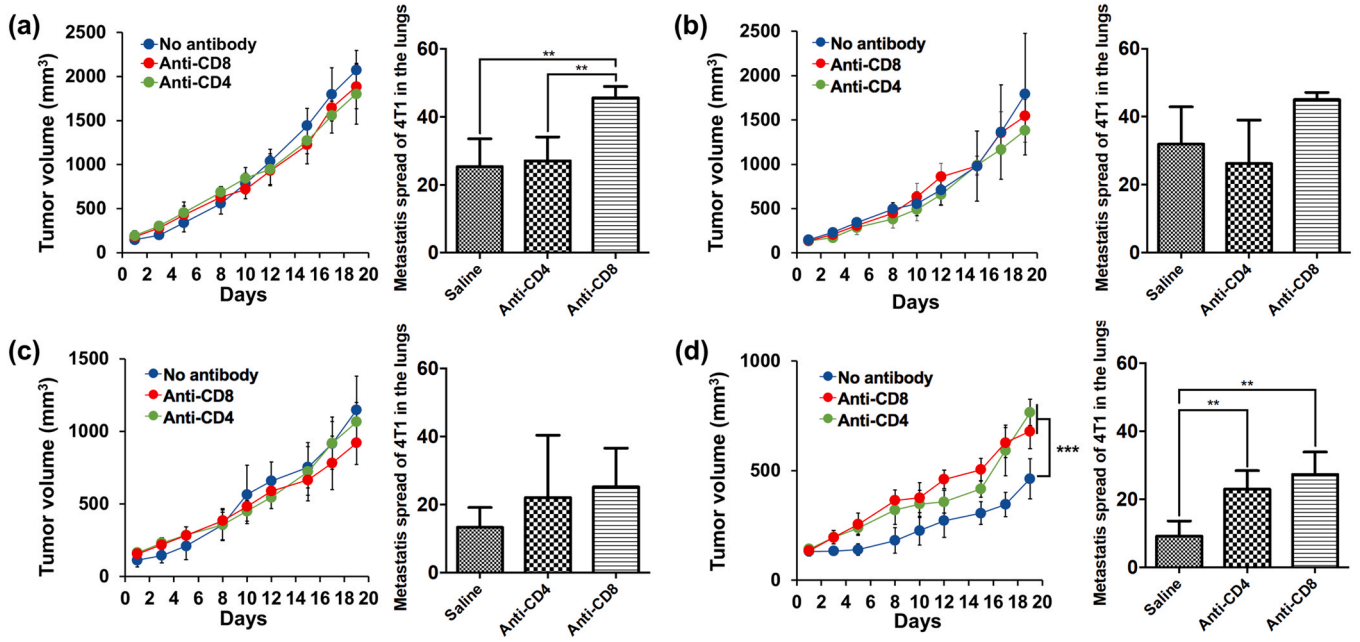

Fig. 8. Effect of CD4⁺ and CD8⁺ cells depletion of the tumor growth curves (left panels) and lung metastasis (right panels) in 4T1 tumor bearing mice treated with: (a) saline, **(b)** POx-PTX (30 mg/kg). **(c)** POx-PTX (75 mg/kg) and **(d)** co-loaded POx-PTX/PLX (75 mg/kg PTX and 75 mg/kg PLX3397). Systemic depletion of $CD4^+$ and $CD8^+$ T cells restores tumor growth in vivo. Mice were treated with CD4 or CD8 depleting antibodies (intraperitoneally (ip) using q4d × 4). Two days after the first injection of an antibody, saline or drugs were administered using q4d × 4 regimen. For the assessment of the metastatic spread, lungs were harvested 24 days after the first sample treatment (Supplementary Fig. S7). Statistical comparisons for tumor inhibition were done using a two-way ANOVA followed by Bonferroni post-tests for multiple comparisons (n = 4–5). Statistical comparisons for lung metastases were analyzed using an unpaired two-tailed t-test. Statistical difference: ** ($p < 0.01$) and *** ($p < 0.001$). (see Supplementary Table S7 for statistical comparisons between all groups).

pathways on cancer cells, as was shown previously [37,38]. We re-confirmed TME-independent PLX3397 cytotoxicity in our tumor cell models and observed strong cytotoxic synergy between PLX3397 and PTX, which provided an additional rationale for combining these two drugs.

The assessment of the changes of the immune cell populations in TME, induction of ICD, and tumor rechallenge experiments suggest that the co-loaded drug combination has the most potent immunotherapeutic effect compared to both single-dose therapies using POx-PLX and POx-PTX. By depleting the $CD4^+$ and $CD8^+$ T cells, we observed partial attenuation of the tumor growth suppression, suggesting involvement of T cell immunity in the anti-cancer effects of POx-PTX/PLX. Moreover, we found that POx-PTX/PLX efficiently suppressed the metastatic spread of TNBC (4T1) toward the lungs. Notably, the high-dose POx-PTX has also shown significant activity in this context. This finding is quite remarkable given previous conflicting reports suggesting that potential involvement of the anti-tumor immune responses by PTX may promote metastases while inhibiting the primary tumor [76,77]. The strong anti-metastatic activity of both POx-PTX and POx-PTX/PLX may be of future clinical significance for management of life-threatening metastasis in breast cancer.

The 4T1 cancer cell line is highly metastatic, so migration from the primary tumor to secondary tumor locations may occur. Since high-dose POx-PTX and POx-PTX/PLX treatments inhibited metastases, it could impact the result of vaccination rechallenge study. However, when we compared the growth rate of the secondary tumor to that of the primary tumor, there was no significant difference, indicating marginal biological interaction between two tumors in vivo. Thus, we believe that the growth inhibition of the secondary tumor was mainly due to cancer-specific systemic immune activation, which was also consistent with the enhancement of ICD markers such as CRT and HMGB1 in vivo.

We acknowledge that the PLX solution administered orally in this study was formulated using a commonly used surfactant rather than an optimized formulation. Therefore, the drug's response may vary depending on the composition of excipients in oral dose formulations. The observed suboptimal therapeutic efficacy when using the oral route may be attributed to poor bioavailability resulting from an inadequately optimized drug. Thus, further comparison in a clinical setting should include optimizing the oral dosage form of PLX3397, which was not the focus of this study. A possible explanation for the lack of synergy between anti-PD-1 and POx-PTX/PLX therapy could be 1) the saturated efficacy of POx-PTX/PLX in a given mouse model, where the addition of anti-PD1 did not exert any therapeutic benefit in the model or 2) the induction of drug resistance in the TNBC mouse model, which may decrease the therapeutic efficacy of anti-PD1 treatment [78–80].

In conclusion, this study adds a new perspective for the chemoimmunotherapy of TNBC using POx polymeric micelles. The results demonstrate that PTX even as a single agent, strongly affects TME and induces long-term immune memory. We suggest that the POx micelle formulation can potentially transform the use of this well-known drug by enabling its high dose therapy. In addition, we demonstrate that combining chemoimmunotherapy using PTX and PLX3397 provides consistent improvement of therapeutic outcomes across several TNBC models. These treatments are associated with the repolarization of the immunosuppressive TME and increased T cell immune responses that contribute to the suppression of both the primary tumor and metastatic disease. Overall, the work provides evidence of the benefit of reformulation and outlines a potential translational path for both PTX and PTX and PLX3397 combination using POx polymeric micelles for the TNBC.

Materials and methods

Materials

Amphiphilic triblock copolymer of poly ($MeOx_{35}$-*b*-$BuOx_{20}$-*b*-$MeOx_{34}$) (M_n = 8.6 kDa, M_w/M_n = 1.15) was synthesized by living

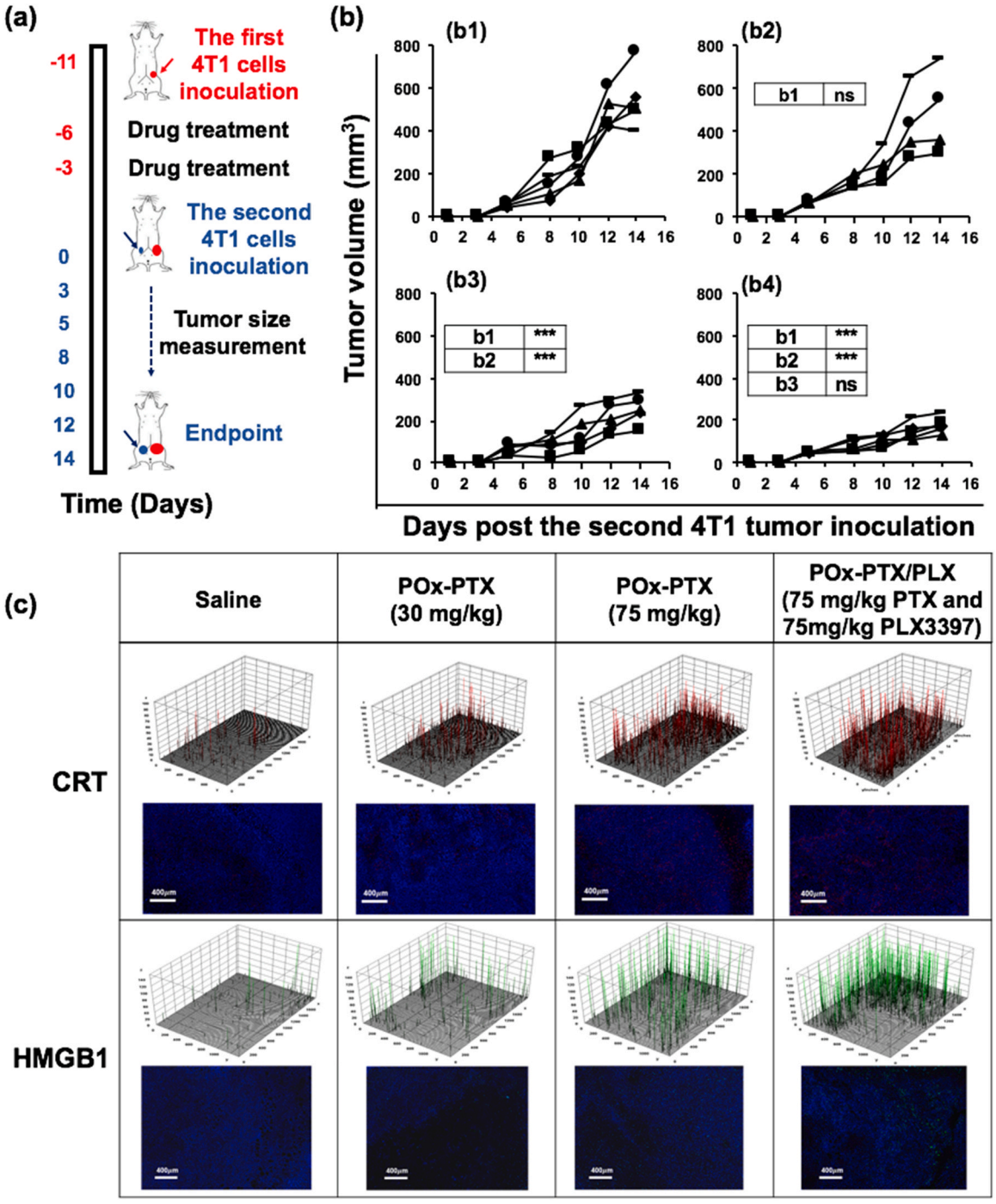

Fig. 9. (a,b) The vaccination-rechallenge experiment and (c) evaluation of ICD in vivo in 4T1 breast tumor model. (a) Scheme of the vaccination protocol and (b) secondary tumor growth after treatment of the primary tumor with (b1) saline, (b2) POx-PTX (30 mg/kg), (b3) POx-PTX (75 mg/kg) and (b4) POx-PTX/PLX (75 mg/kg PTX and 75 mg/kg PLX3397). 4T1 breast cancer cells (10^6 cells) were inoculated into 4th mammary fat pad of BALB/c mice, and when the tumor sizes reached ca. 80–100 mm^3, the animals received saline or drug-loaded micelles iv using q4d × 2 regimen. 3 Days after 2nd dose of treatment, mice were rechallenged with living cancer cells of the same type, inoculated into the contralateral 4th mammary fat pad. The second tumor growth is routinely monitored for 14 days. Statistical difference: $^{*}(p < 0.05)$, $^{**}(p < 0.01)$, and $^{***}(p < 0.001)$. (c) Representative sections of saline or drug-loaded micelles treated tumor, immunostained for 4',6-diamidino-2-phenylindole (DAPI), calreticulin (CRT), and high mobility group box protein 1 (HMGB1). The animals were inoculated with the primary tumor and treated as described above. Tissues were harvested 2 days after the second treatment. Stained signals were visualized by 3D surface plots in Image J.

cationic ring-opening polymerization as described previously [31,32]. Structural properties of POx were determined by ^{1}H NMR spectroscopy (INOVA 400) and gel permeation chromatography (GPCmax VE-2001 system (Viscotek)). PTX was purchased from LC laboratories (Woburn, MA). PLX3397 was purchased from MedKoo Biosciences (Morrisville, NC). All other chemicals were from Fisher Scientific INC. (Fairlawn, NJ) and of analytical grade. 4T1 cells were obtained from UNC Lineberger Tissue Culture Facility. T11-apobec and T12 cells were provided by Dr. Charles M. Perou (Lineberger Comprehensive Cancer Center, Chapel Hill, NC, USA). 4T1 cells were cultured in RPMI medium (11965–092 (Gibco)) supplemented with 10% fetal bovine serum (FBS) and 1% penicillin-streptomycin at 37 ºC in a cell culture incubator. T11-apobec cells were cultured in RPMI medium (11965–092 (Gibco)) supplemented with 5% FBS, 1%

penicillin-streptomycin and puromycin. T12 cells cultured in RPMI medium (11965–092 (Gibco)) supplemented with 5% FBS and 1% penicillin-streptomycin. Anti-mouse PD-1 was purchased from BioXCell (no. BE0146).

Preparation and characterization of drug-loaded polymeric micelle formulations

POx micelle formulations with drugs were prepared by thin-film hydration method as previously described [28,29,31,65]. Briefly, stock solutions of the POx polymer and drugs (PTX and PLX3397) were prepared in absolute ethanol (at 10 mg/ml POx, 5 mg/ml PTX, and 2 mg/ml PLX3397, respectively). These stock solutions were thoroughly mixed at the predetermined ratios based on drug feeding ratio in POx micelles. By completely evaporating ethanol under a stream of inert nitrogen gas, thin films of the drug-polymer homogeneous mixture were obtained. Thin films were subsequently hydrated with sterile saline and incubated (at 70 ºC for POx-PTX (10 min) and POx-PTX/PLX (5 min), and room temperature for POx-PLX (10 min)). The resulting micelle formulations were centrifuged at 10,000 g for 3 min (Sorvall Legend Micro 21 R Centrifuge, Thermo Scientific) to remove any drug precipitates from the micelle formulations. Clear supernatants of the micelle solutions were collected and used for physicochemical analysis of the micelle drugs.

Drug loadings in given micelle drugs were analyzed by high-pressure liquid chromatography (HPLC) system (Agilent Technologies 1200 series) using a Nucleosil C18 column (4.6 mm × 250 mm, 5 µm). A mobile phase composed of water (0.1% trifluoroacetic acid) and acetonitrile (0.1% trifluoroacetic acid) (50/50 vol ratio) was used. Micelle formulations were diluted 50-fold with mobile phase, and 10 µL of diluted micelle samples were injected into the HPLC system for drug loading analysis. The flow rate of the mobile phase was 1.0 ml/min. The detection wavelengths were 270 nm for PLX3397 and 235 nm for PTX. The LE and LC of the micelle formulations were calculated using the following Eqs. (1)–(2).

$$\text{LE (\%)} = (\text{drug mass in micelle}) / (\text{drug mass initially added}) \times 100\ (\%) \quad (1)$$

$$\text{LC (\%)} = (\text{drug mass in micelle}) / (\text{drug mass in micelle + POx mass}) \times 100\ (\%) \quad (2)$$

The size distribution of micelle drugs in solution was measured by Zetasizer Nano ZS (Malvern Instruments Ltd., UK) equipped with a multi-angle sizing option. The effective diameter (D_{eff}) and PDI of each micelle drug were determined by DLS from three measures of three independently prepared micelle drugs. The morphology of POx-PTX/PLX was examined using a LEO EM910 TEM operating at 80 kV (Carl Zeiss SMT Inc., Peabody, MA). Dilute samples of POx-PTX/PLX were attached to copper grid/carbon film and stained with 1% uranyl acetate prior to the TEM imaging. Digital images were obtained using a Gatan Orius SC1000 CCD Digital Camera in combination with Digital Micrograph 3.11.0 software (Gatan Inc., Pleasanton, CA).

The drug release from micelle drugs was investigated using the membrane dialysis method under sink condition [28,29,31,65]. Briefly, micelle drugs were diluted in phosphate-buffered saline (PBS) to achieve 0.1 g/L of total drug concentration in the solution. Then the diluted micelle drug solutions were transferred to floatable Slide-A-Lyzer MINI dialysis devices (100 µL capacity, 10 kDa MWCO) and placed in 30 ml of PBS supplemented with 10% FBS. At predetermined time points, four devices were sacrificed, and micelle drug solutions in the devices were collected. The remaining drugs in the obtained micelle drug samples were quantified by HPLC, as described above. The drug release profiles were plotted by expressing the % drug released from micelle drugs over time.

In vitro cytotoxicity and induction of immunogenic cell death

In vitro cytotoxicity by micelle drugs was determined by measuring cell viability using CCK-8 assay (Dojindo, MD). A 96-well cell culture plates were used to seed 4T1, T11-Apobec, and T12 cells (1×10^4 cells/well) for 24 h at 37 °C in an atmosphere of 5% CO_2 with fresh media. Following 24 h incubation of the TNBC cells in the plates, the cells were treated with micelle drugs of serial dilutions for 48 h. The cells in the plates were then washed with sterile PBS, CCK-8 agents were added to the plates, and the plates were incubated at 37 ºC in an atmosphere of 5% CO_2 for 4 h. The absorbance at 450 nm of each well of the plates was recorded on a UV spectrophotometer (SpectraMax M5, Molecular Devices). Cytotoxicity of micelle drugs on the TNBC cells (expressed as IC_{50}) was analyzed using the GraphPad Prism 7.03 software.

The dead cell apoptosis kit with Annexin V (V13242 (Invitrogen)) was used to analyze the apoptosis and necrosis [81] induced by micelle drugs. 4T1 cells (5×10^4 cells/well) were seeded in 24-well plates and treated with micelle drugs at 1 µg/ml of total drug concentration. After 24 h, the 4T1 cells were harvested and double-stained with Annexin V-FITC and propidium iodide, as mentioned in the product manuals. The apoptotic/necrotic 4T1 cells were analyzed by Attune NxT flow cytometer (Thermo Fisher), and the portions of apoptotic/necrotic 4T1 cells were analyzed using FlowJo v10.4.2 software.

To investigate the induction of ICD in vitro by micelle drug treatment, ICD markers such as ATP and CRT were measured upon treatment of micelle drugs on 4T1 cells. For ATP concentration measurement in vitro, 4T1 cells (1×10^5) were seeded in 24-well plates in fresh media for 24 h, then treated with micelle drugs with serial dilutions for 24 h. Media supernatants of the 4T1 cells in the plates were collected and immediately analyzed with ATPlite one-step luminescence assay kits (PerkinElmer, MA) to measure ATP concentration in the media. To detect CRT translocation to the cell surface by ICD [64], 4T1 cells (1×10^5) were seeded in 24-well plates in fresh media for 24, then treated with micelle drugs with serial dilutions for 24 h. Subsequently, the 4T1 cells in the plates were fixed with 4% formaldehyde and stained with anti-CRT antibody (ab196159 (Abcam)). CRT^+ 4T1 cells were analyzed by Attune NxT flow cytometer (Thermo Fisher), and the percentage of CRT^+ 4T1 cells was analyzed using FlowJo v10.4.2 software.

Determination of MTD

Animal studies were conducted in accordance with the University of North Carolina at Chapel Hill Institutional Animal Care and Use Committee guidelines. MTD of micelle drug (POx-PTX/PLX) was determined by a dose-escalation study using healthy 8-week-old female BALB/c mice (Jackson Laboratory). Mice were randomly divided into five groups and POx-PTX/PLX was administered iv using either q4d × 4 or q4d × 6 regimens. The mice were injected iv with: saline, POx-PTX/PLX (75 mg/kg PTX and 75 mg/kg PLX3397) (iv; q4d × 4), POx-PTX/PLX (100 mg/kg PTX and 100 mg/kg PLX3397) (iv; q4d × 4), POx-PTX/PLX (125 mg/kg PTX and 125 mg/kg PLX3397) (iv; q4d × 4), or POx-PTX/PLX (75 mg/kg PTX and 75 mg/kg PLX3397) (iv; q4d × 6). The body weight change of the mice was monitored every day for 27 days. Drug treatments were discontinued if any signs of toxicity behavior, including hunched posture, rough coat and body weight changes over 15% of the initial body weight.

In vivo TNBC animal models and tumor inhibition studies

Animal studies were conducted in accordance with the University of North Carolina at Chapel Hill Institutional Animal Care and Use Committee guidelines. In order to investigate tumor inhibition by micelle drug treatments, three orthotopic TNBC models

(4T1, T11-apobec, and T12) were employed. Tumor-bearing mouse models were developed as follows. For the 4T1 model, 6–8 weeks old female BALB/c mice (Jackson Laboratory) were orthotopically inoculated in the 4th mammary fat pad with 4T1 cells (1×10^6 cells in 100 µL of PBS and Matrigel (Corning, AZ) mixture (1:1 vol ratio)). For the T11-apobec model, female BALB/c mice (6–8 weeks) were orthotopically inoculated in the 4th mammary fat pad with T11-apobec cells (1×10^5 cells in 100 µL of PBS and Matrigel mixture (1:1 vol ratio)). For the T12 model, female BALB/c mice (6–8 weeks) were orthotopically inoculated in the 4th mammary fat pad with T12 cells (1×10^5 cells in 100 µL of PBS and Matrigel mixture (1:1 vol ratio)). For all breast cancer models, when the tumor sizes reached ca. 100 mm^3, animals were randomized (n = 5) and received the following iv injections via tail vein using q4d × 4 regimen. 1) sterile saline; 2) POx-PTX (30 mg/kg PTX); 3) POx-PLX (75 mg/kg PLX3397); 4) POx-PTX (75 mg/kg PTX); 5) POx-PTX/PLX (30 mg/kg PTX and 30 mg/kg PLX3397), and 6) POx-PTX/PLX (75 mg/kg PTX and 75 mg/kg PLX3397). Tumor size was closely monitored every 2–3 days. Tumor length (L) and width (W) were measured, and tumor volume (V) was calculated using the following equation: $V = ½ \times L \times W^2$. 4T1 tumor-bearing mice were sacrificed on day 21, and tumor and lung samples were collected for IHC analysis. For oral gavage, PLX3397 was solubilized in a mixture of 5% DMSO, 45% PEG300, and 5% Tween 80 in distilled water. For iv administration of free drugs, PTX and PLX3397 were solubilized in the mixture of 50% ethanol and 50% Cremophor and diluted 5 times in PBS before use.

InVivoMAb anti-mouse CD4 (clone GK1.5, BioXCell) or CD8 (clone 2.43, BioXCell) is a monoclonal antibody specific to the CD4 or CD8 antigen on the surface of mouse T cells. The antibody can bind to and effectively deplete CD4-positive or CD8-positive T cells in vivo, decreasing the overall number of T cells. Specifically, for the CD4 + and CD8 + T cell depletion, 4T1 tumor-bearing BABL/c mice were treated with ip injections of an anti-CD4 or anti-CD8 antibody or control saline 2 days before each drug treatment for 4 times in total [60–63].

Actual drug concentration, loading capacity, and loading efficiency of the polymeric micelle formulations for in vivo administration are presented in Table S8**.**

Lung metastasis quantification

Brightfield whole slide images of hematoxylin and eosin-stained lung sections were scanned at 20-fold magnification by the UNC Pathology Services Core (PSC) using the Aperio AT2 digital scanner (Leica Biosystems Imaging, Inc., Deer Park, IL). Digital image analysis was performed by a boarded veterinary pathologist in the UNC PSC using Definiens Architect XD 64 version 2.7.0.60765 to detect tumors within the lung parenchyma. First, lung (ROIs) was detected automatically with a minimum tissue size of 150,000 μm^2, 221 brightness threshold, and 3.6 homogeneity threshold. Large vessels, bronchi, and thymus tissue were manually excluded from the initial ROI. Lung components were segmented into lung, glass (alveolar spaces), blood (erythrocytes in large vessels or alveolar spaces), tumor, and outside lung (glass on the outside of the lung) categories. The resulting lung and blood area (μm^2) for each slide image were added to calculate the total tissue area. The tumor area (μm^2) was then divided by the total tissue area to obtain the tumor percent area. The algorithm was validated by a semi-quantitative assessment of the relative % tumor burden for a subset of the slides.

Flow cytometry

For analyzing the immune cell population changes in the tumors (4T1, T11-apobec, and T12) upon micelle drug treatments, orthotopic primary tumors were harvested 3 days after the second dose. The harvested tumors were enzymatically digested with collagenase (2 mg/ml in Hank's balanced salt solution (HBSS)), dispase (2.5 U/ml in HBSS), and deoxyribonuclease (1 mg/ml in PBS) for 45 min while shaking in an incubator at 37 ºC, and then passed through a 40 μm cell strainer.

The cells were treated with ammonium-chloride-potassium buffer to lyse the red blood cells and dispersed in FACS buffer (2% FBS in PBS solution). Single cell suspensions were counted, and live cells (1×10^6) were stained with a cocktail of fluorescently labeled antibodies for the pre-designed panel (see supplementary Table S4 and S5**)**. Antibodies panel used for flow cytometry are listed in supplementary Table S5. Then the cells were fixed with 4% paraformaldehyde solution and analyzed with Attune NxT flow cytometer (Thermo Fisher, MA) at UNC Flow Cytometry Core Facility. Cell population analysis was performed using FlowJo software (TreeStar, Ashland, OR).

In vivo immunogenic cell death vaccination study

Schematic presentation of the vaccination protocol and drug treatment regimen for the vaccination-rechallenge experiments is described in Fig. 8**(a)**. Briefly, female BALB/c mice (6–8 weeks old) were orthotopically inoculated with 4T1 cells (1×10^6 cells in 100 µL of PBS and Matrigel mixture (1:1 vol ratio)) in the 4th mammary fat pad. When the tumor sizes reached ca. 50–80 mm^3, the animals received the following micelle drugs via iv injections using q4d × 2 regimen. 1) saline; 2) POx-PTX (30 mg/kg PTX); 3) POx-PTX (75 mg/kg PTX); 4) POx-PTX/PLX (75 mg/kg PTX and 75 mg/kg PLX3397). Three days after 2nd dose of treatment, mice were rechallenged with living 4T1 cancer cells of the same type, inoculated into the contralateral 4th mammary fat pad. The second tumor growth was routinely monitored for 14 days. Secondary tumor volume (V) was calculated using the following equation: $V = ½ \times L \times W^2$. Mice were sacrificed on day 14 from the secondary tumor inoculation, and the tumors were collected for IHC analysis. Here, as the first tumor had reached a certain size at approximately 14 days, the mouse was required to be sacrificed in accordance with the animal protocol. Thus, the endpoint was set at day 14. The vaccination rechallenge experiments were also conducted with healthy BALB/c mice (see schematic presentation of the protocol in supplementary Fig. S8**(a)**). Briefly, Healthy mice were treated with saline or POx-PTX/PLX iv using q4d × 2 regimen. Three days after 2nd dose of treatment, mice were challenged with living cancer cells of 4T1 TNBC, inoculated into 4th MFP. The primary tumor growth was routinely monitored for 14 days.

Mouse model intrinsic gene set cluster

mRNAseq data of treatment naïve mouse mammary tumors from Hollern et al. (GEO: GSE124821) [52] and additional data from models presented in this study (GEO: GSE223630) were combined for a total of 232 individual mouse mammary tumors and normal mammary gland controls. New mammary tumor data were processed and sequenced as described by Thennavan et al. [82]. Gene expression of the 232 samples was upper quantile normalized, log2 transformed, and median centered by gene. The dataset was subsequently subset by a 1723-gene human intrinsic gene set [83] based on their mouse homologs. Hierarchical clustering was performed on the final data set with Cluster 3.0 (version 1.59 for Mac OS X). For the clustering, the centered correlation similarity metric was applied, and genes were clustered by centroid linkage. Gene subclusters for luminal, basal, claudin-low and proliferation were selected based on having a Pearson correlation of 0.70 or higher. Visualization of the cluster was conducted with Java TreeView (version 1.2.0 for Mac OS X).

Statistical analysis

GraphPad 6.0 was used for statistical analysis in this study, and numerical results are expressed as mean ± standard deviation in figures and tables. For comparison within two groups, an unpaired two-tailed t-test was used. For comparison among multiple groups, one-way analysis of variance (one-way ANOVA) or two-way ANOVA by Bonferroni post-tests were employed for statistical analysis. Animal survival is presented as Kaplan-Meier survival curves and analyzed via Log-rank (Mantel-Cox) test. The following symbols are presented in the figures to represent the statistical significance: * ($p < 0.05$), ** ($p < 0.01$), *** ($p < 0.001$), and **** ($p < 0.0001$), ns (not significant).

CRediT authorship contribution statement

Chaemin Lim: Conceptualization, Data curation, Methodology, Writing, Visualization. **Duhyeong Hwang**: Conceptualization, Data curation, Methodology, Writing, Visualization. **Mostafa Yazdimamaghani**: Methodology, Validation. **Hannah Marie Atkins**: Methodology, Validation. **Hyesun Hyun**: Methodology, Validation, Writing – review & editing. **Yuseon Shin**: Validation, Writing – review & editing. **Patrick D. Rädler:** Genomic data analysis, writing, Visualization**. Kevin R. Mott: M**ouse tumor collections, data analysis, writing**. Jacob D. Ramsey**: Formal analysis, Investigation. **Charles M. Perou**: Writing – review & editing, Resources. **Marina Sokolsky-Papkov**: Conceptualization, Writing – review & editing, Project administration. **Alexander V. Kabanov**: Conceptualization, Writing – review & editing, Project administration, Funding acquisition.

Data Availability

Data will be made available on request.

Declaration of Competing Interest

A.V.K. is an inventor on patents pertinent to the subject matter of the present contribution, co-founder, stockholder and director of DelAqua Pharmaceuticals Inc. having intent of commercial development of POx based drug formulations. A.V.K. is also a co-founder, stockholder and director of SoftKemo Pharma Corp. and BendaRx Pharma Corp. that develop polymeric drug formulation and a blood cancer drug. M.S.P. discloses potential interest in DelAqua Pharmaceuticals Inc., SoftKemo Pharma Corp. and BendaRx Pharma Corp. as a spouse of co-founder. C.M.P is an equity stockholder and consultant of BioClassifier LLC; C.M.P is also listed as an inventor on patent applications for the Breast PAM50 Subtyping assay.

Acknowledgements

This work was partially supported by the National Cancer Institute (NCI) Alliance for Nanotechnology in Cancer (U54CA198999, Carolina Center of Cancer Nanotechnology Excellence), and NCI's grant R01CA264488 (to AVK). Partial support was also provided by NCI Breast SPORE program (P50-CA058223), and RO1-CA148761 (to CMP). Animal Studies were performed within the UNC Lineberger Animal Studies Core (ASC) Facility at the University of North Carolina at Chapel Hill. YM and HH postdoctoral fellowships were supported through the Carolina Cancer Nanotechnology Training Program funded by NCI (T32CA196589). The UNC Lineberger Animal Studies Core was supported, in part, by an NCI Center Core Support Grant (CA16086) to the UNC Lineberger Comprehensive Cancer Center. The authors thank C. Santos, M. Ross, and A. Valdivia at Animal Studies Core of UNC for helping with the intravenous/intraperitoneal injections. TEM was performed by A. Shankar Kumbhar at the Chapel Hill Analytical and Nanofabrication Laboratory (CHANL), a member of the North Carolina Research Triangle Nanotechnology Network (RTNN), which was supported by the NSF (grant ECCS-1542015) as part of the National Nanotechnology Coordinated Infrastructure (NNCI).

Appendix A. Supporting information

Supplementary data associated with this article can be found in the online version at doi:10.1016/j.nantod.2023.101884.

References

[1] B.P. Schneider, E.P. Winer, W.D. Foulkes, J. Garber, C.M. Perou, A. Richardson, G.W. Sledge, L.A. Carey, Clin. Cancer Res 14 (2008) 8010–8018.
[2] R. Dent, M. Trudeau, K.I. Pritchard, W.M. Hanna, H.K. Kahn, C.A. Sawka, L.A. Lickley, E. Rawlinson, P. Sun, S.A. Narod, Clin. Cancer Res 13 (2007) 4429–4434.
[3] L. Yin, J.J. Duan, X.W. Bian, S.C. Yu, Breast Cancer Res. 22 (2020) 61.
[4] C. Denkert, C. Liedtke, A. Tutt, G. von Minckwitz, Lancet 389 (2017) 2430–2442.
[5] R. Nanda, L.Q. Chow, E.C. Dees, R. Berger, S. Gupta, R. Geva, L. Pusztai, K. Pathiraja, G. Aktan, J.D. Cheng, V. Karantza, L. Buisseret, J. Clin. Oncol.: Off. J. Am. Soc. Clin. Oncol. 34 (2016) 2460–2467.
[6] N.G. Adel, Am. J. Manag Care 27 (2021) S87–S96.
[7] S.K. Bunt, L. Yang, P. Sinha, V.K. Clements, J. Leips, S. Ostrand-Rosenberg, Cancer Res. 67 (2007) 10019–10026.
[8] A.P. Cogdill, M.C. Andrews, J.A. Wargo, Br. J. Cancer 117 (2017) 1–7.
[9] S. Spranger, T.F. Gajewski, Oncoimmunology 5 (2016) e1086862.
[10] N.A. Taylor, S.C. Vick, M.D. Iglesia, W.J. Brickey, B.R. Midkiff, K.P. McKinnon, S. Reisdorf, C.K. Anders, L.A. Carey, J.S. Parker, C.M. Perou, B.G. Vincent, J.S. Serody, J. Clin. Investig. 127 (2017) 3472–3483.
[11] J. Zhou, X.H. Wang, Y.X. Zhao, C. Chen, X.Y. Xu, Q. Sun, H.Y. Wu, M. Chen, J.F. Sang, L. Su, X.Q. Tang, X.B. Shi, Y. Zhang, Q. Yu, Y.Z. Yao, W.J. Zhang, J. Cancer 9 (2018) 4635–4641.
[12] G.W. Tormoen, M.R. Crittenden, M.J. Gough, Adv. Radiat. Oncol. 3 (2018) 520–526.
[13] A.K. Mehta, E.M. Cheney, C.A. Hartl, C. Pantelidou, M. Oliwa, J.A. Castrillon, J.R. Lin, K.E. Hurst, M. de Oliveira Taveira, N.T. Johnson, W.M. Oldham, M. Kalocsay, M.J. Berberich, S.A. Boswell, A. Kothari, S. Johnson, D.A. Dillon, M. Lipschitz, S. Rodig, S. Santagata, J.E. Garber, N. Tung, J. Yelamos, J.E. Thaxton, E.A. Mittendorf, P.K. Sorger, G.I. Shapiro, J.L. Guerriero, Nat. Cancer 2 (2021) 66–82.
[14] H. Zheng, S. Siddharth, S. Parida, X. Wu, D. Sharma, Cancers 13 (2021).
[15] C. Medrek, F. Ponten, K. Jirstrom, K. Leandersson, BMC Cancer 12 (2012) 306.
[16] Z.Y. Yuan, R.Z. Luo, R.J. Peng, S.S. Wang, C. Xue, Onco Targets Ther. 7 (2014) 1475–1480.
[17] P. Tymoszuk, P. Charoentong, H. Hackl, R. Spilka, E. Muller-Holzner, Z. Trajanoski, P. Obrist, F. Revillion, J.P. Peyrat, H. Fiegl, W. Doppler, BMC Cancer 14 (2014) 257.
[18] Y. Lan, D. Zhang, C. Xu, K.W. Hance, B. Marelli, J. Qi, H. Yu, G. Qin, A. Sircar, V.M. Hernandez, M.H. Jenkins, R.E. Fontana, A. Deshpande, G. Locke, H. Sabzevari, L. Radvanyi, K.M. Lo, Sci. Transl. Med. 10 (2018).
[19] B. Ruffell, N.I. Affara, L.M. Coussens, Trends Immunol. 33 (2012) 119–126.
[20] P. Pathria, T.L. Louis, J.A. Varner, Trends Immunol. 40 (2019) 310–327.
[21] L. Gao, F.Q. Wang, H.M. Li, J.G. Yang, J.G. Ren, K.F. He, B. Liu, W. Zhang, Y.F. Zhao, Oncotarget 7 (2016) 87037–87051.
[22] D.G. DeNardo, D.J. Brennan, E. Rexhepaj, B. Ruffell, S.L. Shiao, S.F. Madden, W.M. Gallagher, N. Wadhwani, S.D. Keil, S.A. Junaid, H.S. Rugo, E.S. Hwang, K. Jirstrom, B.L. West, L.M. Coussens, Cancer Discov. 1 (2011) 54–67.
[23] C.H. Ries, M.A. Cannarile, S. Hoves, J. Benz, K. Wartha, V. Runza, F. Rey-Giraud, L.P. Pradel, F. Feuerhake, I. Klaman, T. Jones, U. Jucknischke, S. Scheiblich, K. Kaluza, I.H. Gorr, A. Walz, K. Abiraj, P.A. Cassier, A. Sica, C. Gomez-Roca, K.E. de Visser, A. Italiano, C. Le Tourneau, J.P. Delord, H. Levitsky, J.Y. Blay, D. Ruttinger, Cancer Cell 25 (2014) 846–859.
[24] S.L. Shiao, B. Ruffell, D.G. DeNardo, B.A. Faddegon, C.C. Park, L.M. Coussens, Cancer Immunol. Res 3 (2015) 518–525.
[25] A. Osipov, M.T. Saung, L. Zheng, A.G. Murphy, J. Immunother. Cancer 7 (2019) 224.
[26] J.B. Epstein, J. Thariat, R.J. Bensadoun, A. Barasch, B.A. Murphy, L. Kolnick, L. Popplewell, E. Maghami, CA Cancer J. Clin. 62 (2012) 400–422.
[27] F. Schettini, M. Giuliano, S. De Placido, G. Arpino, Cancer Treat. Rev. 50 (2016) 129–141.
[28] X. Wan, J.J. Beaudoin, N. Vinod, Y. Min, N. Makita, H. Bludau, R. Jordan, A. Wang, M. Sokolsky, A.V. Kabanov, Biomaterials 192 (2019) 1–14.
[29] X. Wan, Y. Min, H. Bludau, A. Keith, S.S. Sheiko, R. Jordan, A.Z. Wang, M. Sokolsky-Papkov, A.V. Kabanov, ACS Nano 12 (2018) 2426–2439.
[30] N. Vinod, D. Hwang, S.H. Azam, A.E.D. Van Swearingen, E. Wayne, S.C. Fussell, M. Sokolsky-Papkov, C.V. Pecot, A.V. Kabanov, Bio Protoc. 11 (2021) e3959.
[31] R. Luxenhofer, A. Schulz, C. Roques, S. Li, T.K. Bronich, E.V. Batrakova, R. Jordan, A.V. Kabanov, Biomaterials 31 (2010) 4972–4979.
[32] Y. Seo, A. Schulz, Y. Han, Z. He, H. Bludau, X. Wan, J. Tong, T.K. Bronich, M. Sokolsky, R. Luxenhofer, R. Jordan, A.V. Kabanov, Polym. Adv. Technol. 26 (2015) 837–850.

[33] C. Lim, J.D. Ramsey, D. Hwang, S.C.M. Teixeira, C.-D. Poon, J.D. Strauss, E.P. Rosen, M. Sokolsky-Papkov, A.V. Kabanov, Small 18 (2022) 2103552.
[34] A. Schulz, S. Jaksch, R. Schubel, E. Wegener, Z. Di, Y. Han, A. Meister, J. Kressler, A.V. Kabanov, R. Luxenhofer, C.M. Papadakis, R. Jordan, ACS Nano 8 (2014) 2686–2696.
[35] M. Grüne, R. Luxenhofer, D. Iuga, S.P. Brown, A.-C. Pöppler, J. Mater. Chem. B 8 (2020) 6827–6836.
[36] D. Hwang, J.D. Ramsey, A.V. Kabanov, Adv. Drug Deliv. Rev. 156 (2020) 80–118.
[37] P.P. Patwardhan, O. Surriga, M.J. Beckman, E. de Stanchina, R.P. Dematteo, W.D. Tap, G.K. Schwartz, Clin. Cancer Res 20 (2014) 3146–3158.
[38] A. Galanis, M. Levis, Haematologica 100 (2015) e77–e79.
[39] Y. Liu, K.S. Given, E.L. Dickson, G.P. Owens, W.B. Macklin, J.L. Bennett, Exp. Neurol. 318 (2019) 32–41.
[40] R. Wesolowski, N. Sharma, L. Reebel, M.B. Rodal, A. Peck, B.L. West, A. Marimuthu, P. Severson, D.A. Karlin, A. Dowlati, M.H. Le, L.M. Coussens, H.S. Rugo, Ther. Adv. Med Oncol. 11 (2019) 1758835919854238.
[41] T.C. Chou, P. Talalay, Adv. Enzym. Regul. 22 (1984) 27–55.
[42] C.J. Aslakson, F.R. Miller, Cancer Res. 52 (1992) 1399–1405.
[43] I. Sagiv-Barfi, H.E. Kohrt, D.K. Czerwinski, P.P. Ng, B.Y. Chang, R. Levy, Proceedings of the National Academy of Sciences of the United States of America, 112 (2015) E966-E972.
[44] A. Filatenkov, J. Baker, A.M. Muller, G.O. Ahn, H. Kohrt, S. Dutt, K. Jensen, S. Dejbakhsh-Jones, R.S. Negrin, J.A. Shizuru, E.G. Engleman, S. Strober, Radiat. Res. 182 (2014) 163–169.
[45] F. Meyer-Losic, S.P. Newman, J.M. Day, M.J. Reed, P.G. Kasprzyk, A. Purohit, P.A. Foster, PloS One 8 (2013) e80305.
[46] D.P. Hollern, N. Xu, A. Thennavan, C. Glodowski, S. Garcia-Recio, K.R. Mott, X. He, J.P. Garay, K. Carey-Ewend, D. Marron, J. Ford, S. Liu, S.C. Vick, M. Martin, J.S. Parker, B.G. Vincent, J.S. Serody, C.M. Perou, Cell 179 (2019) 1191–1206 e1121.
[47] A.D. Pfefferle, Y.N. Agrawal, D.C. Koboldt, K.L. Kanchi, J.I. Herschkowitz, E.R. Mardis, J.M. Rosen, C.M. Perou, Dis. Model Mech. 9 (2016) 749–757.
[48] A.D. Pfefferle, J.I. Herschkowitz, J. Usary, J.C. Harrell, B.T. Spike, J.R. Adams, M.I. Torres-Arzayus, M. Brown, S.E. Egan, G.M. Wahl, J.M. Rosen, C.M. Perou, Genome Biol. 14 (2013) R125.
[49] J.I. Herschkowitz, W. Zhao, M. Zhang, J. Usary, G. Murrow, D. Edwards, J. Knezevic, S.B. Greene, D. Darr, M.A. Troester, S.G. Hilsenbeck, D. Medina, C.M. Perou, J.M. Rosen, Proc. Natl. Acad. Sci. USA 109 (2012) 2778–2783.
[50] S. Singh, N. Lee, D.A. Pedroza, I.L. Bado, C. Hamor, L. Zhang, S. Aguirre, J. Hu, Y. Shen, Y. Xu, Y. Gao, N. Zhao, S.H. Chen, Y.W. Wan, Z. Liu, J.T. Chang, D. Hollern, C.M. Perou, X.H.F. Zhang, J.M. Rosen, Cancer Res 82 (2022) 2281–2297.
[51] Z. He, X. Wan, A. Schulz, H. Bludau, M.A. Dobrovolskaia, S.T. Stern, S.A. Montgomery, H. Yuan, Z. Li, D. Alakhova, Biomaterials 101 (2016) 296–309.
[52] D.P. Hollern, N. Xu, A. Thennavan, C. Glodowski, S. Garcia-Recio, K.R. Mott, X. He, J.P. Garay, K. Carey-Ewend, D. Marron, J. Ford, S. Liu, S.C. Vick, M. Martin, J.S. Parker, B.G. Vincent, J.S. Serody, C.M. Perou, Cell 179 (2019) 1191–1206 e1121.
[53] P. Kaur, G.M. Nagaraja, H. Zheng, D. Gizachew, M. Galukande, S. Krishnan, A. Asea, BMC Cancer 12 (2012) 1–12.
[54] B. Schrörs, S. Boegel, C. Albrecht, T. Bukur, V. Bukur, C. Holtsträter, C. Ritzel, K. Manninen, A.D. Tadmor, M. Vormehr, Front. Oncol. 10 (2020) 1195.
[55] T. Sørlie, C.M. Perou, R. Tibshirani, T. Aas, S. Geisler, H. Johnsen, T. Hastie, M.B. Eisen, M. Van De Rijn, S.S. Jeffrey, Proceedings of the National Academy of Sciences, 98 (2001) 10869–10874.
[56] K. Dias, A. Dvorkin-Gheva, R.M. Hallett, Y. Wu, J. Hassell, G.R. Pond, M. Levine, T. Whelan, A.L. Bane, PloS One 12 (2017) e0168669.
[57] C.M. Perou, T. Sørlie, M.B. Eisen, M. Van De Rijn, S.S. Jeffrey, C.A. Rees, J.R. Pollack, D.T. Ross, H. Johnsen, L.A. Akslen, nature 406 (2000) 747–752.
[58] A. Prat, J.S. Parker, O. Karginova, C. Fan, C. Livasy, J.I. Herschkowitz, X. He, C.M. Perou, Breast Cancer Res. 12 (2010) 1–18.
[59] S. Bissinger, C. Hage, V. Wagner, I.P. Maser, V. Brand, M. Schmittnaegel, A.M. Jegg, M. Cannarile, C. Watson, I. Klaman, N. Rieder, A. Gonzalez Loyola, T.V. Petrova, P.A. Cassier, C. Gomez-Roca, V. Sibaud, M. De Palma, S. Hoves, C.H. Ries, Sci. Transl. Med 13 (2021).
[60] K.N. Balogh, D.J. Templeton, J.V. Cross, PloS One 13 (2018) e0197702.
[61] J. Li, Y. Lee, Y. Li, Y. Jiang, H. Lu, W. Zang, X. Zhao, L. Liu, Y. Chen, H. Tan, Immunity, 48 (2018) 773–786 e775.
[62] K.D. Moynihan, C.F. Opel, G.L. Szeto, A. Tzeng, E.F. Zhu, J.M. Engreitz, R.T. Williams, K. Rakhra, M.H. Zhang, A.M. Rothschilds, Nat. Med. 22 (2016) 1402–1410.
[63] C. Vanpouille-Box, J.M. Diamond, K.A. Pilones, J. Zavadil, J.S. Babb, S.C. Formenti, M.H. Barcellos-Hoff, S. Demaria, Cancer Res. 75 (2015) 2232–2242.
[64] J. Humeau, S. Levesque, G. Kroemer, J.G. Pol, Methods Mol. Biol. 1884 (2019) 297–315.
[65] Z. He, X. Wan, A. Schulz, H. Bludau, M.A. Dobrovolskaia, S.T. Stern, S.A. Montgomery, H. Yuan, Z. Li, D. Alakhova, M. Sokolsky, D.B. Darr, C.M. Perou, R. Jordan, R. Luxenhofer, A.V. Kabanov, Biomaterials 101 (2016) 296–309.
[66] T.S. Lau, L.K.Y. Chan, G.C.W. Man, C.H. Wong, J.H.S. Lee, S.F. Yim, T.H. Cheung, I.A. McNeish, J. Kwong, Cancer Immunol. Res 8 (2020) 1099–1111.
[67] M. Jiang, J. Zeng, L. Zhao, M. Zhang, J. Ma, X. Guan, W. Zhang, Nanoscale 13 (2021) 17218–17235.
[68] F. Meng, J. Wang, Y. He, G.M. Cresswell, N.A. Lanman, L.T. Lyle, T.L. Ratliff, Y. Yeo, Proc. Natl. Acad. Sci. USA 119 (2022) e2122595119.
[69] D.V. Krysko, A.D. Garg, A. Kaczmarek, O. Krysko, P. Agostinis, P. Vandenabeele, Nat. Rev. Cancer 12 (2012) 860–875.
[70] L. Milane, M. Amiji, Drug Deliv. Transl. Res. 11 (2021) 1309–1315.
[71] A. Khurana, P. Allawadhi, I. Khurana, S. Allwadhi, R. Weiskirchen, A.K. Banothu, D. Chhabra, K. Joshi, K.K. Bharani, Nano Today 38 (2021) 101142.
[72] C.W. Wanderley, D.F. Colon, J.P.M. Luiz, F.F. Oliveira, P.R. Viacava, C.A. Leite, J.A. Pereira, C.M. Silva, C.R. Silva, R.L. Silva, C.A. Speck-Hernandez, J.M. Mota, J.C. Alves-Filho, R.C. Lima-Junior, T.M. Cunha, F.Q. Cunha, Cancer Res 78 (2018) 5891–5900.
[73] D. Miles, J. Gligorov, F. Andre, D. Cameron, A. Schneeweiss, C. Barrios, B. Xu, A. Wardley, D. Kaen, L. Andrade, V. Semiglazov, M. Reinisch, S. Patel, M. Patre, L. Morales, S.L. Patel, M. Kaul, T. Barata, J. O'Shaughnessy, I.M. investigators, Ann. Oncol. 32 (2021) 994–1004.
[74] D. Hwang, N. Vinod, S.L. Skoczen, J.D. Ramsey, K.S. Snapp, S.A. Montgomery, M. Wang, C. Lim, J.E. Frank, M. Sokolsky-Papkov, Z. Li, H. Yuan, S.T. Stern, A.V. Kabanov, Biomaterials 278 (2021) 121140.
[75] H. Gelderblom, M.V. de Sande, Future Oncol. 16 (2020) 2345–2356.
[76] L. Volk-Draper, K. Hall, C. Griggs, S. Rajput, P. Kohio, D. DeNardo, S. Ran, Cancer Res 74 (2014) 5421–5434.
[77] S. Ran, Cancer Res. 75 (2015) 2405–2410.
[78] M.L. Ascierto, A. Makohon-Moore, E.J. Lipson, J.M. Taube, T.L. McMiller, A.E. Berger, J. Fan, G.J. Kaunitz, T.R. Cottrell, Z.A. Kohutek, Clin. Cancer Res. 23 (2017) 3168–3180.
[79] Q. Lei, D. Wang, K. Sun, L. Wang, Y. Zhang, Front. Cell Dev. Biol. 8 (2020) 672.
[80] J.-Y. Sun, D. Zhang, S. Wu, M. Xu, X. Zhou, X.-J. Lu, J. Ji, Biomark. Res. 8 (2020) 1–10.
[81] M.S. D'Arcy, Cell Biol. Int. 43 (2019) 582–592.
[82] A. Thennavan, S. Garcia-Recio, S. Liu, X. He, C.M. Perou, npj Breast Cancer 8 (2022) 83.
[83] J.S. Parker, M. Mullins, M.C.U. Cheang, S. Leung, D. Voduc, T. Vickery, S. Davies, C. Fauron, X. He, Z. Hu, J.F. Quackenbush, I.J. Stijleman, J. Palazzo, J.S. Marron, A.B. Nobel, E. Mardis, T.O. Nielsen, M.J. Ellis, C.M. Perou, P.S. Bernard, J. Clin. Oncol. 27 (2009) 1160–1167.